UNIVERSITEIT VAN PRETORIA
UNIVERSITY OF PRETORIA
YUNIBESITHI YA PRETORIA

ON CHANNEL ESTIMATION FOR MOBILE WIMAX

By

Waldo Kleynhans

Studyleader: Prof J.C Olivier

Submitted in partial fulfillment of the requirements for the degree

Master of Engineering (Electronic)

in the

Department of Electrical, Electronic and Computer Engineering

in the

School of Engineering

in the

Faculty of Engineering, Built Environment and Information Technology

UNIVERSITY OF PRETORIA

July 2008

SUMMARY

ON CHANNEL ESTIMATION FOR MOBILE WIMAX
by
Waldo Kleynhans
Studyleader: Prof J.C Olivier
Department of Electrical, Electronic and Computer Engineering
Master of Engineering (Electronic)

In mobile communication channels information symbols are transmitted through a communication channel that is prone to fading and multipath propagation. At the receiver, the effect of multipath propagation is reduced by a process called channel equalization. Channel equalization relies on an accurate estimate of the channel state information (CSI). This estimate is obtained using a channel estimation algorithm. Mobile WiMAX is a recently released technology that makes use of an orthogonal frequency division multiplexing (OFDM) based physical layer to transmit information over a wireless communication channel. In this dissertation, frequency and time domain channel estimation methods typically used in classical OFDM systems, using block and comb type pilot insertion schemes, were analyzed and adopted for mobile WiMAX. Least squares (LS) and linear minimum mean square error (LMMSE) channel estimation methods were considered in the case of block type pilot insertion. In the case of comb type pilot insertion, piecewise constant, linear, spline cubic as well as discrete Wiener interpolation methods were considered. A mobile WiMAX simulation platform was developed as part of the dissertation to evaluate and compare the performance of these different channel estimation methods. It was found that the performance of the channel estimation methods, applied to a real world mobile WiMAX simulation platform, conforms to the expected performance of the corresponding classical OFDM channel estimation methods found in literature.

Keywords:
Channel estimation, CSI, LS, LMMSE, mobile WiMAX, OFDM.

UNIVERSITEIT VAN PRETORIA
UNIVERSITY OF PRETORIA
YUNIBESITHI YA PRETORIA

SAMEVATTING

KANAAL ESTIMASIE VIR MOBIELE WIMAX

deur

Waldo Kleynhans

Studieleier: Prof J.C Olivier

Departement Elektriese, Elektroniese en Rekenaar Ingenieurswese

Meester in Ingenieurswese (Elektronies)

In mobiele kommunikasie kanale word informasie beïnvloed deur onder andere sein verswakking en multipad propagasie. By die ontvanger word die effek van die kanaal verminder deur kanaal vereffening. Kanaal vereffening maak gebruik van kanaal toestand informasie (KTI). Die akkuraatheid van die KTI het ’n groot impak op die effektiwiteit van die vereffenaar. Die KTI word verkry deur gebruik te maak van ’n kanaal estimasie algoritme. Mobiele WiMAX is ’n nuwe tegnologie wat gebruik maak van ortogonale frekwensie divisie multipleksering (OFDM) op die fisiese vlak om data simbole te stuur deur n draadlose kommunikasie kanaal. In hierdie disertasie word frekwensie en tyd vlak kanaal estimasie metodes wat op klassieke OFDM stelsels gebruik word geanaliseer in die geval van blok en kam tipe verwysing simbool invoeging skemas. Least Squares (LS) en linear minimum mean square error (LMMSE) kanaal estimasie metodes was gebruik in die geval van blok tipe verwysing simbool invoeging skemas. In die geval van kam tipe verwysing simbool invoeging was stuksgewyse konstante, liniêre, spline cubic en diskrete Wiener interpolasie metodes gebruik. As deel van hierdie studie was ’n mobile WiMAX simulator ontwikkel om die uitvoering van die kanaal estimasie metodes met mekaar te vergelyk. Daar was gevind dat die uitvoering van hierdie metodes, toegepas op ’n regte wêreld simulasie platform, in lyn is met verwagte resultate in die literatuur.

Sleutelwoorde:

Kanaal estimasie, KTI, mobiele WiMAX, OFDM.

This dissertation is dedicated to:

God Almighty, for all the countless opportunities that He has given me;

My loving family and friends, for their support, encouragement and good advice

UNIVERSITEIT VAN PRETORIA
UNIVERSITY OF PRETORIA
YUNIBESITHI YA PRETORIA

ACKNOWLEDGEMENT

The author would like to thank the following people and institutions without whose help this dissertation would not have been possible:

- My study leader Prof J.C Olivier, for all the advice and guidance he has given me throughout the course of my studies.
- The Center for Teletraffic Engineering in an Information Society (CeTEIS) for their financial support.
- Sunil Maharaj, Lynette Van den Heever and my fellow students at the Sentech Chair in Broadband Wireless Multimedia Communications (BWMC) at the University of Pretoria for making me feel part of the research team.
- My fellow student Brian Salmon for his useful suggestions and advice.
- The University of Pretoria's computer clusters maintained by Hans Grobler which greatly aided in my simulations.

CONTENTS

LIST OF FIGURES

LIST OF TABLES

ABBREVIATIONS

First Generation	1G
Second Generation	2G
Third Generation	3G
Fourth Generation	4G
Adaptive Modulation	AM
Advanced Modulation and Coding	AMC
Advanced Mobile Phone System	AMPS
Access Point	AP
Additive White Gaussian Noise	AWGN
Bit Error Rate	BER
Belief Propagation	BP
Convolutional Code	CC
Code Division Multiple Access	CDMA
Channel Impulse Response	CIR
Cyclic Prefix	CP
Channel State Information	CSI
Convolutional Turbo Code	CTC
Channel Transfer Function	CTF
Discrete Fourier Transform	DFT
Downlink	DL
Differential Phase-Shift Keying	DPSK
Digital Subscriber Loop	DSL
Enhanced Data Rate for GSM Evolution	EDGE
Evolution Data-Optimized	EVDO
Fast Fourier Transform	FFT

Frequency Domain	FD
Frequency Division Duplexing	FDD
Full-Duplex Frequency Division Duplexing	FD-FDD
Frequency Division Multiple Access	FDMA
Frequency Pilot Time Average	FPTA
Fully Used Sub-Channelization	FUSC
General Packet Radio Service	GPRS
Global System Mobile	GSM
Half-Duplex Frequency Division Duplexing	HD-FDD
High-Speed Downlink Packet Access	HSDPA
Inter Symbol Interference	ISI
Kanaal Toestant Informasie	KTI
Low Density Parity Check Code	LDPC
Line of Sight	LOS
Least Squares	LS
Metropolitan Area Network	MAN
Multiple Input Multiple Output	MIMO
Mean Square	MS
Mean Square Error	MSE
Most Significant Taps	MST
Nordic Mobile Telephone	NMT
Orthogonal Frequency Division Multiplexing	OFDM
Piecewise Constant	PC
Power Delay Profile	PDP
Probability Density Function	PDF
Pseudo Noise	PN
Pilot Symbol Assisted Modulation	PSAM
Partially Used Sub-Channelization	PUSC
Quadrature Amplitude Modulation	QAM
Radio Frequency	RF
Signal-to-Noise Ratio	SNR
Scalable Orthogonal Frequency Division Multiple Access	S-OFDMA

Total Access Communication System	TACS
Time Domain	TD
Time Division Duplexing	TDD
Time Division Multiplexed	TDM
Time Division Multiple Access	TDMA
Uplink	UL
Universal Mobile Telecommunication System	UMTS
Wireless Ethernet Compatibility Alliance	WECA
Worldwide Interoperability for Microwave Access	WiMAX
Wireless Local Area Network	WLAN

CHAPTER ONE
INTRODUCTION

Since Guglielmo Marconi first demonstrated wireless communication over water in 1897, wireless communications have been adopted with great enthusiasm across the world. In recent times the radio communications industry has grown by orders of magnitude mainly due to advances in RF circuit fabrication making large scale deployment of radio communication networks more affordable and easy to use [1].

1.1 BRIEF HISTORY OF CELLULAR COMMUNICATION

The development of the cellular concept by Bell Laboratories in the 1960s and 1970s [2, 3] revolutionized personal communications around the world. The number of cellular users worldwide grew from 25000 in 1984 to roughly 25 million in 1993. Since then the number of cellular telephone subscribers have increased in excess of 50% per year [1]. First generation (1G) cellular systems were only capable of transmitting analog voice information. The most prominent 1G systems are advanced mobile phone system (AMPS), Nordic mobile telephone (NMT) and total access communication system (TACS). The development of second generation (2G) networks were driven by a need to improve transmission quality, coverage and system capacity. Advances in technology enabled 2G to use digital transmission. The most popular 2G technology is global system mobile (GSM) [1] which uses time division multiple access (TDMA)/frequency division duplexing (FDD) multiple access techniques. 2G standards were initially designed before widespread use of the internet and consequently uses circuit switched data modems which limits download speed and increases the cost because a data session will typically be billed for the time that the connection is active rather than the amount of data that is received.

Because of the higher demand for data services, data-centric services were developed that could be overlaid on existing 2G technologies [1] which in the case of TDMA systems included general packet radio service (GPRS) and enhanced data rate for GSM evolution (EDGE). This "improved" 2G technology is commonly referred to as 2.5G.

As the internet grew more popular, so did the demand for higher rate internet services. This instigated the development of third generation (3G) wireless networks. Universal mobile telecommunication system (UMTS) and code division multiple access (CDMA) 2000 are the two main technologies in the 3G arena and provides users with a downlink (DL) speed of up to 384 Kb/s and 144 Kb/s respectively. Evolution data-optimized (1xEVDO) as well as high-speed downlink packet access (HSDPA), which is an enhancement of CDMA2000 and UMTS respectively, has made it possible for users to achieve up to 4.9 Mbps using a 1.25 MHz channel and 14 Mbps using a 5 MHz channel respectively [4].

Fourth generation (4G) is the next generation of wireless networks and is expected to replace 3G networks sometime in the future. 4G is intended to provide high speed, high capacity and low cost per bit IP based services. The goal of 4G is to replace the current core cellular networks with a single worldwide cellular core network standard based on IP for data, video as well as voice services [5].

1.2 WIRELESS LOCAL AREA NETWORKS

In the previous section, a brief overview of cellular wireless communications was given. It was shown that when cellular technology was initially designed, the need for data services were not really a priority because the internet was still in its infancy. When considering a wireless local area network (WLAN), the design objectives were completely different to that of cellular communications. In 1987 the IEEE 802.11 Wireless LAN task group was founded to begin standardization of spread spectrum WLAN's for use in license free bands. The focus of WLAN's is on high data throughput rather than mobility. IEEE 802.11 was standardized in 1997 and offered user data rates of 2Mbps [1]. Since the initial release of the 802.11 standard, several supplementary standards were added which includes the 802.11a and 802.11b standard respectively. The 802.11a standard has been named Wi-Fi by the wireless ethernet compatibility alliance (WECA) and provides up to 54 Mbps in the 5 GHz band [6].

Although WLAN's are able to provide high speed connectivity in an office environment where the distance between the user and access point (AP) is tens of meters, there still exist a need for users to connect over larger areas. For this reason the IEEE802.16 MAN (metropolitan area network) (commonly known as WiMAX) task group aimed to develop a wireless access technology that is able to

	802.16	**802.16-2004**	**802.16e-2005**
Spectrum (GHz)	10-66	<11	<6
Line of sight required?	yes	no	no
Throughput (Mbps)	32-134	≤ 75	≤ 15
Modulation	QPSK, 16QAM, 64QAM	QPSK, 16QAM, 64QAM	QPSK, 16QAM, 64QAM
Bandwidth (MHz)	20, 25, 28	Scalable [1.25,20]	Scalable [1.25,20]
Handover capability	no	no	yes
Mobility	fixed	nomadic	fully mobile

TABLE 1.1: WiMAX parameters

support high throughput broadband connections over long distances for portable, nomadic and mobile users.

1.3 WIMAX

The WiMAX standard was developed by the WiMAX forum [7]. The WiMAX standard is based on the IEEE802.16 MAN standard and consists of three key physical layer profiles namely WirelessMAN-SC, WirelessMAN-OFDM and WirelessMAN-OFDMA. These physical layer profiles are generally associated with the IEEE 802.16, 802.16-2004 and 802.16e-2005 standards respectively. Table 1.1 gives some of the specifications for these three profiles [8]. The 802.16 standard is mainly used for microwave back haul and requires line of sight (LOS) while the 802.16-2004 and 802.16e-2005 (often referred to as *mobile WiMAX*) does not require LOS and can be used for broadband access. The main difference between the 802.16-2004 and 802.16e-2005 standard is the mobility and handover capability. The 802.16-2004 standard does not have any support for handovers and is generally referred to as a fixed broadband application supporting very little (nomadic) mobility. The 802.16e-2005 standard on the other hand has handover support making it a fully mobile standard.

When considering cellular and WLAN technologies, there exists a gap between the mobility offered by cellular technologies and the potential throughput offered by WLAN. Mobile WiMAX can potentially be the technology to bridge this divide as shown in Figure 1.1. Although mobile WiMAX is not considered to be a 4G technology, its high spectral efficiency and all IP core is in line with the design methodology envisaged to be used in future 4G systems.

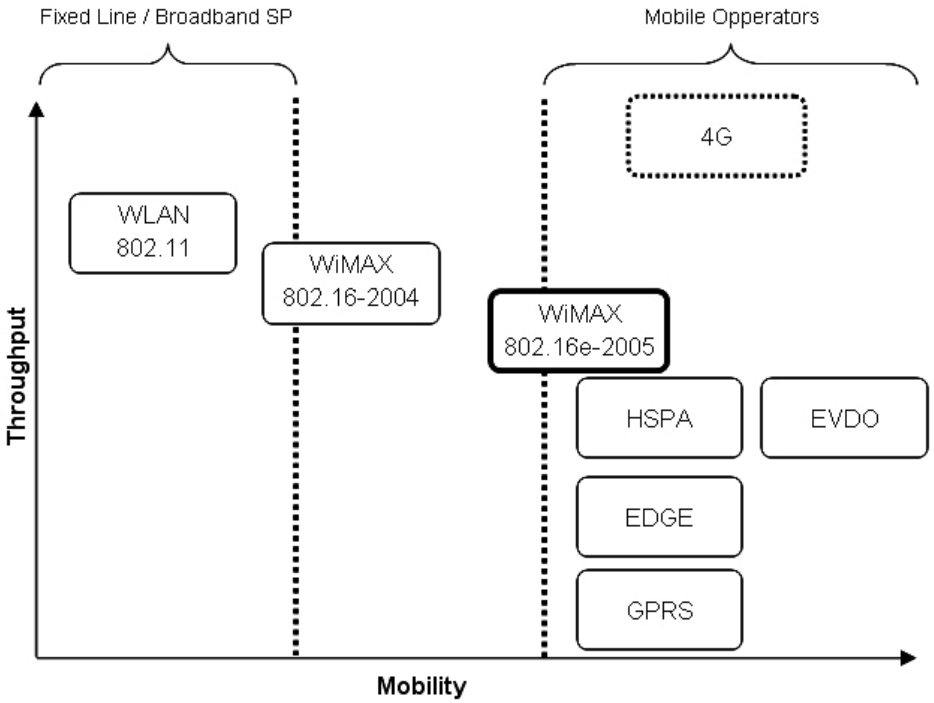

FIGURE 1.1: Mobility versus Throughput

The multiplexing/access method used in mobile WiMAX is scalable orthogonal frequency division multiple access (S-OFDMA) [9] which is based on the principle of orthogonal frequency division multiplexing (OFDM). OFDM is a form of multicarrier transmission and divides a single bit stream into a series of interleaved bit streams which is then modulated over several carriers. The concept of multicarrier transmission was used more than 30 years ago [10], and has been of continuing interest ever since.

In recent times a worldwide convergence has occurred for the use of OFDM as an emerging technology for high data rates. In particular, three WLAN systems in three regions of the world: the USA (IEEE 802.11a), Europe (ETSI BRAN HIPERLAN/2) and Japan (ARIB MMAC), respectively have adopted OFDM as the modulation scheme of choice.

1.4 CHANNEL ESTIMATION FOR OFDM SYSTEMS

Using differential phase-shift keying (DPSK) in OFDM alleviates the need for estimation and tracking of the mobile channel, but also limits the transmission speed and results in a 3 dB loss with regards to the signal-to-noise ratio (SNR) [11]. When using coherent modulation, arbitrary signal constellations can be used, but channel estimation is required for coherent detection. It follows that channel

estimation is important when considering coherent OFDM type systems. If mobility is high, the channel changes much faster and consequently, channel estimates need to be updated more frequently. As will be shown in the following chapters of this dissertation, the coherence time, which is the time that the channel is regarded to be invariant, will be an important parameter when considering channel estimation in a mobile environment.

1.5 OBJECTIVE OF THIS DISSERTATION

Numerous channel estimation methods for OFDM systems can be found in the literature. Quite often, an apples to apples comparison of these methods are difficult when considering the fact that simulations are done under various channel conditions using independent simulation platforms. This motivated the development of a mobile WiMAX simulation platform to test and evaluate various OFDM channel estimation methods.

As shown in Figure 1.1, mobile WiMAX aims to provide high data rates in a fully mobile environment. Unlike classical OFDM based broadband technologies like Wi-Fi and HIPERLAN which operates in a fixed environment, mobile WiMAX is prone to rapid channel fluctuations induced by higher mobility. This implies that channel estimation methods will have to be adapted to operate in an environment where the channel changes rapidly. The need for accurate channel estimation is crucial when performing coherent demodulation. In the case of OFDMA, an accurate channel estimate can be used not only to do equalization but also to increase capacity by using techniques like pre-coding, subcarrier allocation and adaptive modulation.

The objective of this dissertation is to apply a number of different types of classical OFDM channel estimation methods based on generic pilot insertion schemes to mobile WiMAX. The aim is to evaluate these methods and compare them using a mobile WiMAX simulation platform to be developed as part of this dissertation. The simulator is required to be developed in accordance with the 802.16e-2005 standard [9] and needs to simulate channel impairments caused by noise and frequency selective Rayleigh fading [12].

1.6 OUTLINE OF THE DISSERTATION

In chapter 2, an analysis is done on OFDM where the importance of channel estimation is shown analytically. Chapter 3 gives an overview of mobile WiMAX and also discusses the mobile WiMAX simulation platform. The different classical OFDM channel estimation methods based on comb and

block type pilot insertion is shown in chapter 4 where the application of each of the channel estimation methods to mobile WiMAX is also discussed. The performance results of the different mobile WiMAX channel estimation methods are given in chapter 5. The dissertation is concluded in chapter 6 with concluding remarks and future research.

1.7 CONTRIBUTIONS

The following conference papers were written for submission to the *IEEE Personal, Indoor and Mobile Radio Communications (PIMRC)* 2008 conference and was based on results directly obtained from this study:

1. W. Kleynhans, B.P. Salmon, J.C. Olivier and B.T. Maharaj, "On Adaptive Frequency Domain Interpolation for Mobile WiMAX", submitted for publication.

2. W. Kleynhans, B.P. Salmon, J.C. Olivier and B.T. Maharaj, "An Evaluation of Channel Estimation Methods on a Mobile WiMAX Platform", submitted for publication.

The author co-authored the following paper that was written for submission to the *IEEE PIMRC* 2008 conference and was based on a related study on the performance of coding techniques in a mobile WiMAX system with reduced transmission power:

1. B.P. Salmon, W. Kleynhans, J.C. Olivier and B.T. Maharaj, "Performance Analysis of Channel Coding Techniques in a Mobile WiMAX System with Reduced Transmission Power", submitted for publication.

The following journal paper was based on the mobile WiMAX simulation platform and was submitted to *IEEE Transactions on Education*:

1. B.P. Salmon, W. Kleynhans, J.C. Olivier and B.T. Maharaj, "Teaching the Theory of Channel Estimation and Coding via a Mobile WiMAX Simulation Platform", submitted for publication.

The following journal papers were published. This research was based on a related study that utilized a GSM simulation platform developed by the author:

1. J.C. Olivier, W. Kleynhans and S. Miteff, "Teaching the theory of estimation and detection via a GSM radio interface Simulation", *IEEE Transactions on Education*, vol. 49, pp. 61 - 66, Feb 2006.

2. J.C. Olivier and W. Kleynhans, "Single antenna interference cancellation for synchronised GSM networks using a widely linear receiver", *IET Transactions on Communications*, vol. 1, pp. 61 - 66, Feb 2007.

CHAPTER TWO

ORTHOGONAL FREQUENCY DIVISION MULTIPLEXING

OFDM is a particular form of multi-carrier transmission and is suited for frequency selective channels and high data rates. This technique transforms a frequency-selective wide-band channel into a group of frequency non-selective narrow band channels which makes it robust against large delay spreads by preserving orthogonality in the frequency domain. Moreover, the introduction of cyclic redundancy known as a cyclic prefix (CP) at the transmitter reduces the complexity to only fast Fourier transform (FFT) processing and one tap scalar equalization at the receiver [13].

The history of multi-carrier modulation began more than 30 years ago. At the beginning, only analog design based on the use of orthogonal waveforms was proposed [14]. The use of the discrete Fourier transform (DFT) for modulation and demodulation was first proposed in [15]. Only recently has it been finding its way into commercial use, as the recent developments in technology have lowered the cost of the signal processing that is needed to implement OFDM systems.

The aim of this chapter is to give an overview of the functional blocks that make up a typical OFDM system which includes the transmitter, channel and receiver as shown in Figure 2.1. The importance of channel estimation is shown analytically and serves as a framework for the channel estimation methods to be presented in the following chapters.

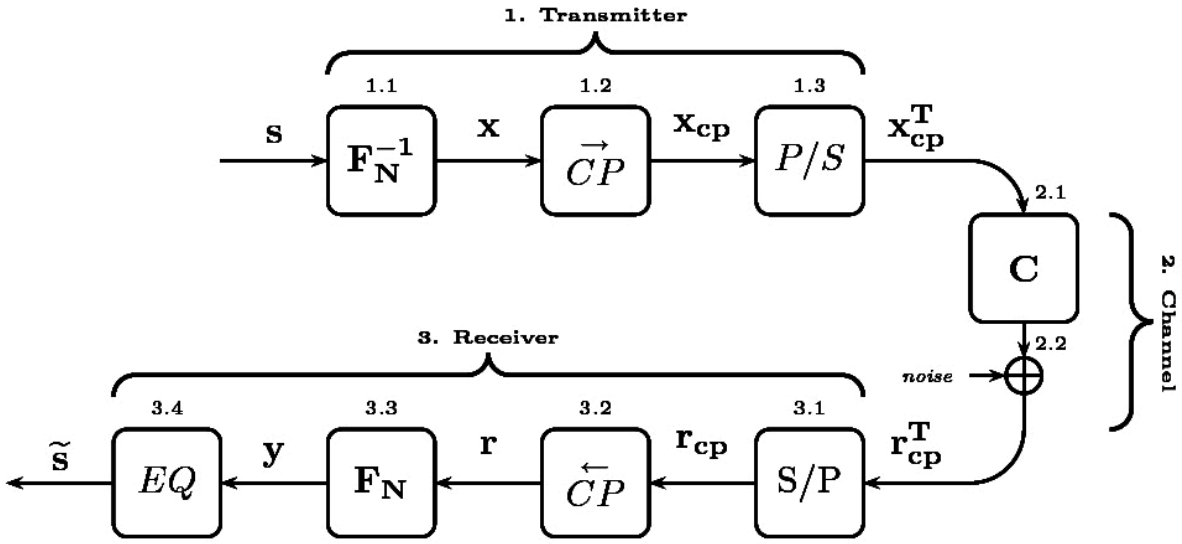

FIGURE 2.1: OFDM model

2.1 TRANSMITTER

The transmitter include blocks *1.1*, *1.2* and *1.3* as shown in Figure 2.1. A block of N symbols is transmitted, this model assumes that the symbols that are to be transmitted are already encoded and modulated. The block of symbols $\mathbf{s} = [s_1\ s_2\ ...\ s_N]^T$ has to be transformed to the time domain (TD) before transmission. This is done by multiplying $\mathbf{s}$ by the inverse DFT matrix $\mathbf{F}_N^{-1}$ *(block 1.1)* to yield the time domain block vector $\mathbf{x} = [x_1\ x_2\ ...\ x_N]^T$. The DFT matrix $\mathbf{F}_N$ is a $N \times N$ matrix defined as

$$\mathbf{F}_N(r,c) = \left[\frac{1}{\sqrt{N}}\, e^{\frac{-2\pi i}{N}}\right]^{(r-1)\cdot(c-1)}, \tag{2.1}$$

where $\mathbf{F}_N(r,c)$ is the value of row r and column c of the $\mathbf{F}_N$ matrix [16]. Once in the TD, $\mathbf{x}$ has to be appended with a CP of length d *(block 1.2)*. The CP is merely the last d symbols of the TD block $\mathbf{x}$ appended to the beginning of the frame as shown in Figure 2.2 [17].

In Figure 2.2, the useful symbol time is denoted as T_b and the time associated with the CP duration, often referred to as the guard time, is denoted as T_g. The entire symbol duration is indicated as T_s. It should be noted that the transmitter energy increases with the length of the guard time while the receiver energy remains the same [17]. This results in a loss when considering $\frac{E_b}{N_0}$ of

$$\left(\frac{E_b}{N_0}\right)_{loss\ (dB)} = 10\ log\left(\frac{T_b}{T_s}\right). \tag{2.2}$$

The guard time T_g should be greater or equal to the channel delay spread [13]. The addition of the CP

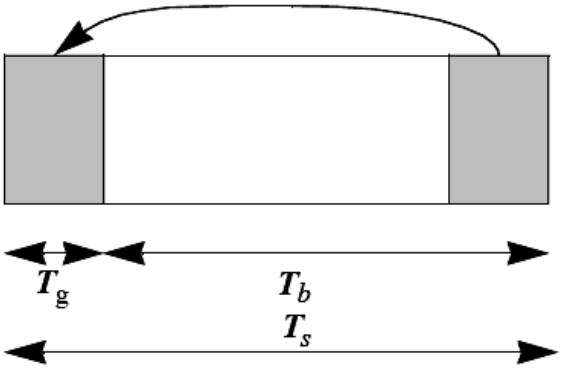

FIGURE 2.2: Cyclic prefix addition (taken from [17] page 494 figure 213)

allows the channel effect to be circularized, the importance of this will become more transparent when discussing the receiver. It is important to mention the fact that the channel should remain invariant for the entire symbol duration T_s to be able to circularize the convolution [18]. A parallel to serial conversion *(block 1.3)* is performed on $\mathbf{x_{cp}}$ before transmission over the channel.

2.2 CHANNEL

The mobile wireless channel is one of the most prominent factors that inhibits the performance of wireless communication systems. The radio wave propagation between the transmitter and receiver is dramatically influenced by the environmental surroundings and can vary from simple line of sight to severe obstruction caused by buildings, mountains, foliage etc. The signal strength at the receiver can be characterized in two ways namely small scale and large scale fading [1]. Large scale fading is mainly attributed to the distance, obstruction and relative height between the transmitter and receiver whereas small scale fading can be influenced by a number of physical factors which includes the relative speed between the transmitter and the receiver as well as the transmission bandwidth of the signal. This dissertation will only address the small scale fading effects of the mobile channel. The interested reader is referred to [1, 19] for more information regarding the effects of large scale fading.

2.2.1 STATISTICS OF SMALL SCALE FADING

When a received signal is made up of multiple reflective rays and has a significant line of sight component, the envelope amplitude can be characterized by a Rician probability density function (PDF) and is appropriately referred to as Rician fading [19]. The Rician PDF approaches a Rayleigh distribution when no line of sight component is present. Most mobile radio systems operate in urban

Tap	Relative delay [ns]	Average Power [dB]
1	0	0
2	310	-1
3	710	-9
4	1090	-10
5	1730	-15
6	2510	- 20

TABLE 2.1: Example of a tapped-delay line profile

environments where a line of sight component is usually non existent [1]. For the remainder of this dissertation, it is thus assumed that the loss in SNR due to fading follows a Rayleigh PDF described as

$$p(r) = \begin{cases} \frac{r}{\sigma^2} exp\left(-\frac{r^2}{2\sigma^2}\right), & for\ r \geq 0 \\ 0, & otherwise \end{cases}, \tag{2.3}$$

where r is the envelope amplitude and σ^2 is the time average power of the received signal [19].

2.2.2 THE MULTIPATH CHANNEL

Multipath propagation occurs when multiple versions of the same signal arrives at the receiver at different time instances and can be characterized by the power delay profile (PDP). The PDP is represented as a plot of the relative received power as a function of the excess delay and is modeled as a tapped-delay line profile [1]. Table 2.1 gives an example of a tapped-delay line profile used to model a vehicular test environment operating in the 2 GHz region [20]. The characteristics of a multipath channel can be modeled by approximating the channel impulse response (CIR).

2.2.3 FREQUENCY SELECTIVE RAYLEIGH FADING

In section 2.2.2 it was shown that the effect of multipath can be modeled by means of a CIR. In this dissertation it is assumed that each of the taps undergo independent Rayleigh fading governed by the statistics given in section 2.2.1. If the CIR consists of only a single tap, the system experiences no inter symbol interference (ISI) which implies that the channel response over all the frequency components are the same. This type of fading is commonly referred to as flat fading [19].

In the case of multiple taps, certain frequency components of the received signal are faded differently than others and is commonly referred to as frequency selective fading. The complex baseband

representation of a frequency selective Rayleigh fading channel can be described by

$$c(t,\tau) = \sum_{k=0}^{L} \gamma_k(t)\delta(\tau - \tau_k) \ , \tag{2.4}$$

where τ_k is the delay of the kth tap and $\gamma_k(t)$ is the corresponding complex amplitude [21]. If it is assumed that the path delays are sample spaced with $L+1$ channel taps, (2.4) can be written in vector form as

$$\mathbf{c} = [\overbrace{c_0}^{\gamma_0}, \overbrace{c_1}^{\gamma_1}, \overbrace{c_2}^{\gamma_2}, ..., \overbrace{c_L}^{\gamma_L}] \ . \tag{2.5}$$

The channel waveform γ_k is modeled as a wide-sense stationary complex Gaussian process with zero mean. The marginal distribution of the phase is uniform with the amplitude having a Rayleigh distribution *(see section 2.2.1)*. The autocorrelation properties of the random process γ_k are governed by the Doppler frequency f_D [22] and can be expressed as

$$\mathbf{R}_{\gamma_k\gamma_k} = J_o(2\pi f_D \tau) \ , \tag{2.6}$$

where $J_o()$ is the zero-order Bessel function. As stated previously, it is assumed that all the γ_k's are independent for different paths. Assuming that the length of the transmitted vector is $Z = N + d$, the channel matrix $\mathbf{C}$ shown in *block 2.1* of Figure 2.1 has the following form

$$\mathbf{C} = \underbrace{\begin{bmatrix} c_0 & 0 & \dots & \dots & \dots & \dots & 0 \\ c_1 & c_0 & 0 & \dots & \dots & \dots & \vdots \\ c_2 & \ddots & \ddots & \ddots & \ddots & \ddots & \vdots \\ \vdots & \ddots & \ddots & \ddots & \ddots & \ddots & \vdots \\ c_L & \ddots & \ddots & \ddots & \ddots & \ddots & 0 \\ \vdots & \ddots & \ddots & \ddots & \ddots & \ddots & 0 \\ 0 & \dots & c_L & \dots & c_2 & c_1 & c_0 \end{bmatrix}}_{Z \times Z} \ . \tag{2.7}$$

2.2.4 ADDITIVE WHITE GAUSSIAN NOISE

The noise shown in *block 2.2* could originate from a verity of sources which includes, galactic noise, amplifier noise as well as thermal noise. The resultant noise is known as additive white Gaussian noise (AWGN) and has a zero mean Gaussian distribution with the PDF

$$\rho(n) = \frac{1}{\sqrt{2\pi}\sigma_n} e^{-\frac{n^2}{2\sigma_n^2}} \ , \tag{2.8}$$

where σ_n^2 is the variance of the noise [11].

2.3 RECEIVER

At the receiver side, a serial to parallel conversion is done on the received time block *(block 3.1)* and the CP of d symbols is removed at the receiver *(block 3.2)*. Assuming that the channel has $L+1$ taps and the CP length is greater than the CIR length ($d \geq L$), the received sequence after removing the CP can be expressed as

$$\underbrace{\begin{bmatrix} r_1 \\ r_2 \\ \vdots \\ r_N \end{bmatrix}}_{\mathbf{r}} = \underbrace{\begin{bmatrix} c_L & \dots & \dots & c_0 & 0 & \dots & 0 \\ 0 & c_L & \dots & \dots & c_0 & \ddots & \vdots \\ \vdots & \ddots & \ddots & \ddots & \ddots & \ddots & 0 \\ 0 & \dots & 0 & c_L & \dots & \dots & c_0 \end{bmatrix}}_{\mathbf{C}} \underbrace{\begin{bmatrix} x_{N-L+1} \\ \vdots \\ x_N \\ x_1 \\ x_2 \\ \vdots \\ x_N \end{bmatrix}}_{\mathbf{x_{cp}}}, \tag{2.9}$$

where $\mathbf{r} = [r_1\ r_2\ ...\ r_N]^T$ is the received sequence of length N. $\mathbf{C}$ is the $N \times N+L$ channel matrix with $[c_0\ c_1\ ...\ c_L]$ being the symbol spaced channel tap coefficients. The transmitted block with CP is indicated as $\mathbf{x_{cp}}$. For the sake of completeness, it is shown that the length of the CP has to be

$$\begin{aligned} N + d &\geq N + L \\ d &\geq L\,. \end{aligned} \tag{2.10}$$

Adding the CP to the transmitted block has effectively enabled (2.9) to be written as

$$\underbrace{\begin{bmatrix} r_1 \\ r_2 \\ r_3 \\ \vdots \\ \vdots \\ \vdots \\ r_N \end{bmatrix}}_{\mathbf{r}} = \underbrace{\begin{bmatrix} c_0 & 0 & \dots & c_L & c_{L-1} & \dots & c_1 \\ c_1 & c_0 & 0 & \dots & c_L & \dots & c_2 \\ \vdots & \ddots & \ddots & \ddots & \ddots & \ddots & \vdots \\ \vdots & \ddots & \ddots & \ddots & \ddots & \ddots & \vdots \\ c_L & \dots & c_2 & c_1 & c_0 & \dots & 0 \\ \vdots & \ddots & \ddots & \ddots & \ddots & \ddots & 0 \\ 0 & \dots & c_L & \dots & c_2 & c_1 & c_0 \end{bmatrix}}_{\tilde{\mathbf{C}}} \underbrace{\begin{bmatrix} x_1 \\ x_2 \\ x_3 \\ \vdots \\ \vdots \\ \vdots \\ x_n \end{bmatrix}}_{\mathbf{x}}. \tag{2.11}$$

From (2.11) it can be seen that the received vector $\mathbf{r}$ is now a product of the circulant matrix $\widetilde{\mathbf{C}}$ of dimension $N \times N$ and the transmitted vector $\mathbf{x}$. The received symbol has to be transformed back into the Fourier domain *(block 3.3)* which implies that

$$\mathbf{y} = \mathbf{F}_N \mathbf{r} \, . \tag{2.12}$$

Substituting (2.11) into (2.12) yields

$$\mathbf{y} = \mathbf{F}_N \widetilde{\mathbf{C}} \mathbf{x} \, . \tag{2.13}$$

It can be seen from Figure 2.1 that $\mathbf{x}$ is the inverse Fourier transform of $\mathbf{s}$. The received vector $\mathbf{y}$ can thus be written as

$$\mathbf{y} = \mathbf{F}_N \widetilde{\mathbf{C}} \mathbf{F}_N^{-1} \mathbf{s} \, . \tag{2.14}$$

In this dissertation, the channel is assumed to be slowly time-varying, i.e. the channel is approximately constant during one OFDM symbol, so there is no loss of orthogonality between subcarriers. It is shown in [23] that this assumption holds if the duration of an OFDM symbol without CP is

$$T_b \leq \frac{0.01}{f_d} \, , \tag{2.15}$$

where T_b is the duration of an OFDM symbol without the CP, and f_d is the maximum Doppler frequency defined as

$$f_d = \frac{v f_c}{c} \, . \tag{2.16}$$

In (2.16), f_c is the carrier frequency, v is the mobile speed and c is the speed of light. If the conditions shown in (2.15) are met, the diagonal values of the $\widetilde{\mathbf{C}}$ matrix in (2.11) remains approximately constant and $\widetilde{\mathbf{C}}$ can be classified as a circulant matrix.

It is shown in [24] that every $n \times n$ circulant matrix $\mathbf{A}$ has eigenvectors

$$\mathbf{y}^{(m)} = \frac{1}{\sqrt{n}} [1, e^{-2\pi i m/n}, ..., e^{-2\pi i (n-1)/n}]^T \;\; m = 0, 1, ..., n-1 \, , \tag{2.17}$$

and corresponding eigenvalues

$$\psi_m = \sum_{k=0}^{n-1} a_k e^{-2\pi i m k/n} \, . \tag{2.18}$$

In (2.18), the sequence $\{a_k\}$ corresponds to the first column of the circulant matrix $\mathbf{A}$. The $\mathbf{A}$ matrix can be expressed in the form $\mathbf{A} = \mathbf{U}\mathbf{\Psi}\mathbf{U}^H$, where $\mathbf{U}$ consist of the eigenvectors shown in (2.17) in column order as

$$\mathbf{U} = [\mathbf{y}^{(0)}, \mathbf{y}^{(1)}, ..., \mathbf{y}^{(n-1)}] \,, \tag{2.19}$$

and $\mathbf{\Psi}$ is $diag(\psi_k)$. All circulant matrices share the same eigenvectors which implies that the same matrix $\mathbf{U}$ works for all circulant matrices, and any matrix of the form $\mathbf{A} = \mathbf{U}\mathbf{\Psi}\mathbf{U}^H$ is circulant [24]. It can be seen from (2.17) and (2.19) that the $\mathbf{U}$ matrix has equivalence to the DFT matrix defined in (2.1). When considering (2.18) it is also evident that the eigenvalues ψ_k can be obtained by computing the DFT of the sequence $\{a_k\}$.

It follows that the circulant matrix $\widetilde{\mathbf{C}}$ in (2.14) can be written as

$$\widetilde{\mathbf{C}} = \mathbf{U}\mathbf{\Lambda}\mathbf{U}^H = \mathbf{F}_N\mathbf{\Lambda}\mathbf{F}_N^{-1} \,, \tag{2.20}$$

where $\mathbf{U} = \mathbf{F}_N$ and $\mathbf{\Lambda}$ is a diagonal matrix consisting of the eigenvalues of the $\{\widetilde{c}_k\}$ sequence. It should also be noted that $\mathbf{U}$ is unitary, i.e. $\mathbf{U}^H = \mathbf{U}^{-1}$. As stated previously, the sequence $\{\widetilde{c}_k\}$ is the first column of the circulant matrix $\widetilde{\mathbf{C}}$ and can be written in matrix form as

$$\{\widetilde{c}_k\} = \mathbf{c}_N = [\overbrace{c_0 \; c_1 \; ... \; c_L}^{L+1} \; \overbrace{0 \; ... \; 0}^{N-L}] \,. \tag{2.21}$$

The diagonal matrix $\mathbf{\Lambda}$ can then be expressed as

$$\mathbf{\Lambda} = diag(\mathbf{F}_N\mathbf{c}_N) \,. \tag{2.22}$$

When substituting (2.20) into (2.14), $\mathbf{y}$ can be written as

$$\mathbf{y} = \mathbf{F}_N\mathbf{F}_N\mathbf{\Lambda}\mathbf{F}_N^{-1}\mathbf{F}_N^{-1}\mathbf{s} \,. \tag{2.23}$$

Equation 2.23 can then be effectively reduced to

$$\mathbf{y} = \mathbf{\Lambda}\mathbf{s} \,, \tag{2.24}$$

and can be written in matrix form as

$$\underbrace{\begin{bmatrix} y_1 \\ y_2 \\ y_3 \\ \vdots \\ y_N \end{bmatrix}}_{\mathbf{y}} = \underbrace{\begin{bmatrix} h_1 & 0 & 0 & \dots & 0 \\ 0 & h_2 & 0 & \dots & 0 \\ 0 & 0 & h_3 & \dots & 0 \\ & & & \ddots & \\ 0 & & \dots & & h_N \end{bmatrix}}_{\mathbf{\Lambda}} \underbrace{\begin{bmatrix} s_1 \\ s_2 \\ s_3 \\ \vdots \\ s_N \end{bmatrix}}_{\mathbf{s}} . \tag{2.25}$$

2.4 DISCUSSION

In the previous section is was shown that by appending the last d symbols of the transmitted time domain data block, where $(d \geq L)$ and $L+1$ is the number of sample spaced channel taps, the channel matrix in (2.7) effectively becomes circulant *(see equations 2.9 and 2.11)*. It was then shown that the circulant channel matrix can be written in the form $\mathbf{F}_N \mathbf{\Lambda} \mathbf{F}_N^{-1}$ where $\mathbf{\Lambda}$ is a diagonal matrix consisting of the eigenvalues of the time domain zero padded CIR *(see equations 2.17 to 2.20)*. It follows from (2.23) and (2.24) that the received FD vector $\mathbf{y}$ can be written as the product of a diagonal matrix $\mathbf{\Lambda}$ and the transmitted FD vector $\mathbf{s}$ as

$$\underbrace{\begin{bmatrix} y_1 \\ y_2 \\ y_3 \\ \vdots \\ \vdots \\ \vdots \\ y_N \end{bmatrix}}_{\mathbf{y}} = \mathbf{F}_N \underbrace{\begin{bmatrix} c_0 & 0 & \dots & \mathbf{c_L} & \mathbf{c_{L-1}} & \dots & \mathbf{c_1} \\ \mathbf{c_1} & c_0 & 0 & \dots & \mathbf{c_L} & \dots & \mathbf{c_2} \\ \vdots & \ddots & \ddots & \ddots & \ddots & \ddots & \vdots \\ \vdots & \ddots & \ddots & \ddots & \ddots & \ddots & \vdots \\ \mathbf{c_L} & \dots & \mathbf{c_2} & \mathbf{c_1} & c_0 & \dots & 0 \\ \vdots & \ddots & \ddots & \ddots & \ddots & \ddots & 0 \\ 0 & \dots & \mathbf{c_L} & \dots & \mathbf{c_2} & \mathbf{c_1} & c_0 \end{bmatrix}}_{\widetilde{\mathbf{C}}} \mathbf{F}_N^{-1} \underbrace{\begin{bmatrix} s_1 \\ s_2 \\ s_3 \\ \vdots \\ \vdots \\ \vdots \\ s_N \end{bmatrix}}_{\mathbf{s}} = \underbrace{\begin{bmatrix} h_1 & 0 & 0 & \dots & \dots & \dots & 0 \\ 0 & h_2 & 0 & \dots & \dots & \dots & 0 \\ 0 & 0 & h_3 & \ddots & & & \vdots \\ \vdots & \vdots & \ddots & \ddots & \ddots & & \vdots \\ \vdots & \vdots & & \ddots & \ddots & \ddots & \vdots \\ \vdots & \vdots & & & \ddots & \ddots & 0 \\ 0 & 0 & \dots & \dots & \dots & 0 & h_N \end{bmatrix}}_{\mathbf{\Lambda}} \underbrace{\begin{bmatrix} s_1 \\ s_2 \\ s_3 \\ \vdots \\ \vdots \\ \vdots \\ s_N \end{bmatrix}}_{\mathbf{s}} . \tag{2.26}$$

In (2.26) the multipath elements in the $\widetilde{\mathbf{C}}$ matrix are indicated in bold for illustrative purposes. It can be seen that by combining the decomposition properties of a circulant matrix with the inherent inverse DFT and DFT operations associated with OFDM, the multipath elements in the FD effectively disappear.

The values of $\mathbf{h}$ in (2.26) is the FD channel transfer function (CTF) and corresponds to the eigenvalues of the time domain zero padded CIR $\mathbf{c}_N$ shown in (2.21). The received symbol for an arbitrary carrier

i which includes AWGN noise can thus be written as

$$y_i = h_i s_i + n_i \ , \tag{2.27}$$

where s_i is the transmitted symbol, h_i is the CTF at tone i, y_i is the received vector and n_i is AWGN with zero mean and variance σ_n^2.

From (2.27) it can be seen that a received FD symbol y_i is a function of the transmitted FD symbol s_i the CTF h_i as well as AWGN n_i at an arbitrary carrier i. It can thus be concluded that when considering an OFDM system making use of an adequate length CP in a slow fading environment, each sub-carrier can be regarded as a single tap flat fading channel. The consequent absence of ISI influences equalization *(block 3.4)*. Symbol detection can be performed using the per symbol *maximum a-posteriori probability* (MAP) criterion *(as will be shown in chapter 4)* as apposed to computationally expensive trellis based equalization algorithms like Viterbi [11].

From (2.27) it is clear that an estimate of the CTF at carrier i (h_i) needs to be made at the receiver to perform equalization. As will be shown in the following chapters, the accuracy of the CTF influences the performance of OFDM systems. The CTF is obtained by a process called channel estimation and in the chapters to follow, various channel estimation methods will be compared and analyzed.

2.5 CONCLUSION

In this chapter, an analytical approach was used to show the importance of channel estimation in OFDM systems. The focus of this dissertation is on channel estimation in OFDM systems with particular application to mobile WiMAX. The following chapter will give an overview of the mobile WiMAX technology and will also discuss the mobile WiMAX simulation platform developed as part of this dissertation.

CHAPTER THREE

MOBILE WIMAX PLATFORM

The release of the IEEE 802.16-2004 standard [17] has proved to be a viable cost effective alternative to digital subscriber loop (DSL) services. This standard was ratified in December 2005 to include mobility [9]. Mobile WiMAX is a broadband wireless solution that enables convergence of mobile and fixed broadband networks through a common wide area broadband radio access technology and flexible network architecture [25]. The three physical layer specifications that are included in the IEEE 802.16e-2005 standard are single carrier, OFDM and OFDMA. Because of the inherent scalability of OFDMA, it is widely considered to be the physical layer of choice when considering mobile WiMAX [26]. It follows that OFDMA will be the physical layer specification considered in this dissertation.

As part of this dissertation, a mobile WiMAX simulator based on the IEEE 802.16e-2005 Wireless MAN OFDMA physical layer [9] was developed to test the performance of the channel estimation methods discussed in the following chapters. The following sections will provide a brief overview of the mobile WiMAX physical layer as well as the simulator that was developed.

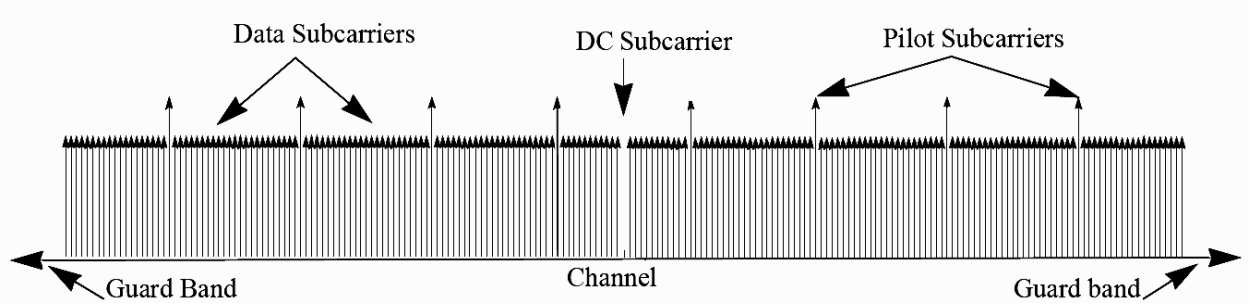

FIGURE 3.1: OFDMA subcarrier structure

3.1 PHYSICAL LAYER DESCRIPTION

3.1.1 OFDMA

In chapter 2, a detailed description of OFDM was given. OFDM is often extended to a multiple access environment using time division multiplexing (TDM) [27] , as is the case with HIPERLAN/2 [28]. An alternative access method to TDM is OFDMA where a number of subcarriers are allocated to a subchannel. Each user is then subsequently assigned one or more subchannels. OFDMA is thus merely a special form of frequency division multiple access (FDMA). The only difference is that all the frequencies are orthogonal resulting in subcarrier frequencies having no interference with one another. In broadband wireless systems the channel has a frequency selective nature. This implies that subcarriers will undergo independent fading. This characteristic can be exploited in OFDMA by employing adaptive modulation (AM) and power adaption methods on individual subcarriers. In [29] the optimality of OFDMA using quadrature amplitude modulation (QAM) was proved.

3.1.2 OFDMA SYMBOL STRUCTURE

The OFDMA symbol consists of three types of carriers which include data symbols which are used to carry the payload information, pilot carriers which are used for channel estimation and synchronization as well as Null carriers which are used for no transmission on the DC carrier and guard bands. Figure 3.1 graphically shows the subcarrier structure of a typical OFDMA symbol [17]. Data carriers are grouped into subsets of subcarriers called subchannels [25]. Pilot allocation is performed differently for different subcarrier allocation modes. The two main subcarrier permutations are *distributed* and *adjacent*. Because of the frequency diversity achieved when using carriers distributed across the entire frequency band, distributed permutations perform very well in mobile applications. Adjacent permutations on the other hand can be properly used for fixed or low mobility environments. The mobile WiMAX physical layer specifies a number of allocation schemes associated with distributed as well as adjacent permutations which includes: fully used sub-channelization (FUSC), partially used

Parameters				
System Bandwidth (MHz)	1.25	2.5	10	20
Sampling Frequency (MHz)	1.4	5.6	11.2	22.4
FFT Size	128	512	1024	2048
Number of Subchannels	2	8	16	32
Subcarrier Frequency Spacing (KHz)	10.94	10.94	10.94	10.94
Useful Symbol Time (μs)	91.4	91.4	91.4	91.4
Guard Time (μs) (CP ratio: $\frac{1}{8}$)	11.4	11.4	11.4	11.4
OFDMA Symbol Duration (μs)	102.9	102.9	102.9	102.9
Number of OFDMA Symbols (5 ms Frame)	48	48	48	48

TABLE 3.1: S-OFDMA parameters

sub-channelization (PUSC) as well as advanced modulation and coding (AMC). DL FUSC uses all the subchannels and achieves frequency diversity by allocating subcarriers across the entire channel bandwidth. Variable as well as fixed pilot sets are used. Fixed pilots are used for all OFDM symbols while variable pilots are divided into subsets which are used in even and odd symbols alternatively [30]. In DL PUSC, sub-channels are divided and assigned to three segments that can be allocated to sectors of the same cell. AMC uses adjacent subcarriers to form subchannels. When fast feedback is used, "water-pouring" type algorithms can be used to enhance the system performance [31, 32].

3.1.3 SCALABLE OFDMA

Mobile WiMAX makes use of the concept of scalable OFDMA (S-OFDMA) which supports a wide range of bandwidths for increased flexibility when considering spectrum allocation. Scalability is achieved by changing the FFT size while keeping the subcarrier frequency spacing constant. Since the symbol time is fixed, the impact on higher functional layers are minimal when adjusting the bandwidth [25]. Table 3.1 shows some of the OFDMA parameters as specified in [9]. The guard time is determined by the CP ratio. The possible guard time values can be $\frac{1}{4}$, $\frac{1}{8}$, $\frac{1}{16}$ and $\frac{1}{32}$ of the length of the OFDMA symbol, the most common CP ratio is $\frac{1}{8}$ and is consequently the only mandatory CP ratio specified in the mobile WiMAX standard [9]. The standard supports various frame sizes but the 5ms frame is the most commonly used.

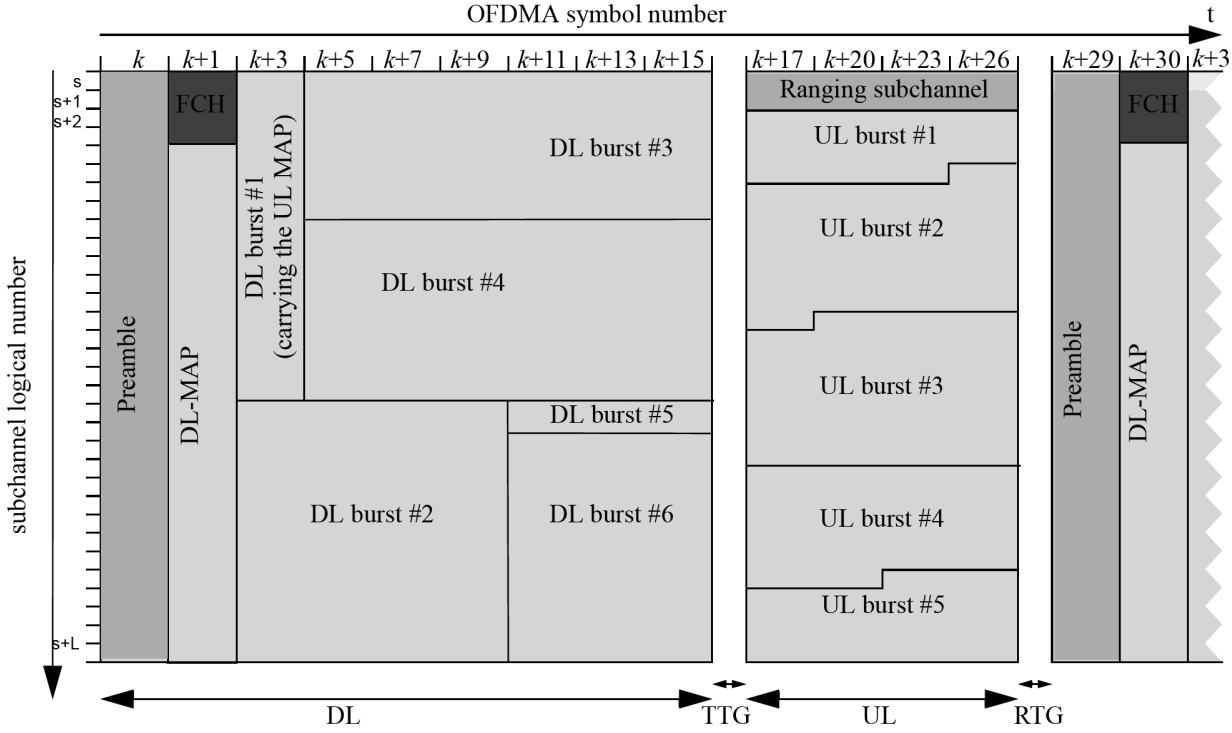

FIGURE 3.2: TDD frame structure (taken from [9] page 357 figure 218)

3.1.4 FRAME STRUCTURE

The mobile WiMAX physical layer supports time division duplexing (TDD), full-duplex frequency division duplexing (FD-FDD) as well as half-duplex FDD (HD-FDD). The initial release of mobile WiMAX certification profiles will however only include TDD [25]. The TDD frame structure is shown in Figure 3.2 where it can be seen that the first symbol that is transmitted is the preamble. The preamble is known *a-priori* at the receiver and is used for channel estimation and equalization. The preamble is followed by the frame control header (FCH) which provides frame configuration information such as the coding scheme. The downlink (DL) and uplink (UL) MAP provides subchannel allocation for the UL and DL frames respectively. UL ranging is used for frequency and power adjustments as well as bandwidth requests.

3.1.5 MODULATION AND CODING

In mobile WiMAX, support for QPSK, 16QAM and 64QAM are mandatory in the DL with 64QAM being optional in the UL. Both convolutional codes and convolutional turbo codes with variable code rates as well as repetition coding are mandatory. Low density parity check codes are supported as an optional feature [25].

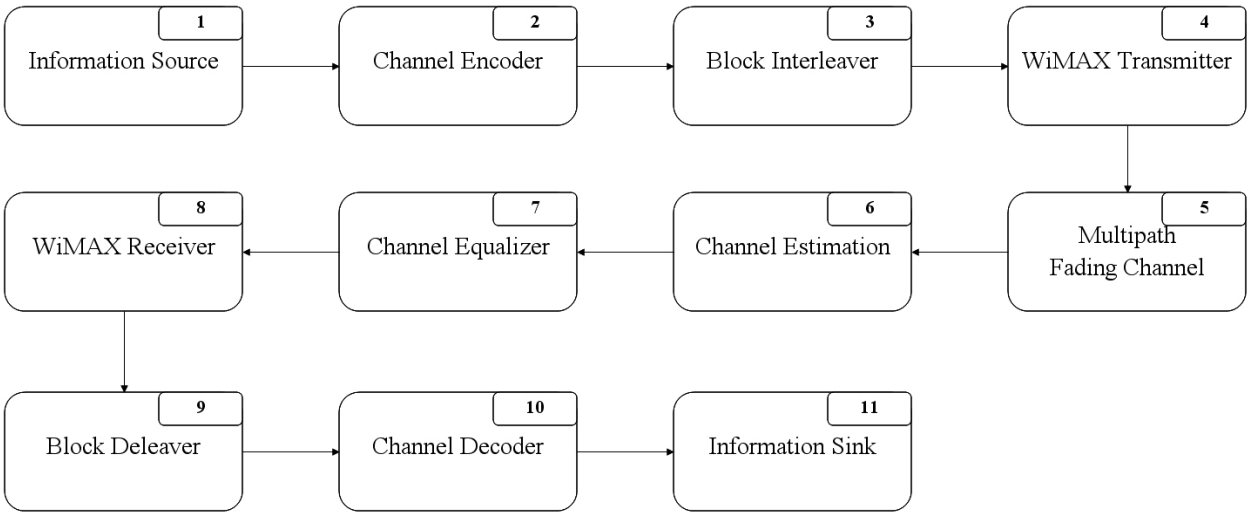

FIGURE 3.3: WiMAX radio interface model used in the simulator

3.2 MOBILE WIMAX RADIO INTERFACE SIMULATOR

The functional layout of the mobile WiMAX physical layer simulator is shown in Figure 3.3. The simulator design was based on the functional blocks shown in Figure 3.3. Each of the blocks were implemented as a C++ object for easy integration.

The source bits are generated by *block 1*. These bits are randomly generated and contain no (negligible) redundancy, which is typical of data produced by source encoding and compression methods. The pseudo-random binary string was generated using the Wichmann-Hill algorithm [33] which is a uniformly distributed random number generator. The payload information bits produced by *block 1* are encoded with a channel encoder *(block 2)* using the standardized mandatory convolutional error control code [9]. The encoded bits are divided into correct block sizes and interleaved in *block 3* in accordance with the WiMAX standard [9] to ensure that faded bits in the transmission sequence are properly distributed over the entire downlink burst. *Block 4* is the WiMAX transmitter, which first modulates the encoded bits obtained from *block 3* in the FD with the user specified modulation schemes which include BPSK, QPSK, 16QAM and 64QAM respectively for each frequency subcarrier. These FD modulated symbols are multiplexed into a OFDMA symbol along with guard bands, pilot symbols and a DC carrier in accordance with the mobile WiMAX standard. The OFDMA symbols are converted into a TD sequence by computing the corresponding IFFT. A CP is appended to the TD OFDMA symbol. The CP length ratio supported includes $\frac{1}{4}$, $\frac{1}{8}$, $\frac{1}{16}$ and $\frac{1}{32}$ of the OFDMA symbol duration.

Block 5 attempts to simulate the effects of a mobile wireless channel. The channel emulates the effect

of either a frequency selective or frequency non-selective fading channel response with correctly scaled AWGN. The radio frequency (RF) signal quality ($\frac{E_b}{N_o}$) can be specified by the user. The ISI is simulated using a channel dispersion profile which can be specified by the user. The dispersion profile for the ITU Ped. B Ch-103 [20] is included in the simulator as a reference *(see Appendix A)*. Each tap of the discrete CIR is assumed to undergo independent Rayleigh fading and is simulated by the improved Jakes model [12]. The rate of fading is determined by selecting the appropriate carrier frequency and mobile velocity.

The receiver attempts to determine the CTF of the channel by means of channel estimation methods *(block 6)*. The DL burst contains a preamble symbol followed by a number of data symbols as seen in Figure 3.2. Data symbols contains both pilot and data carriers, while the preamble contains only pilot carriers. The TD channel estimate is done prior to cyclic prefix removal and FFT transformation while the FD channel estimate is done after the aforementioned. *Block 7* attempts to mitigate the effects of multipath propagation by using the channel estimate obtained in *block 6*. As was shown in chapter 2, single tap frequency domain equalization can be used if the CIR remains constant over the duration of the transmitted OFDMA symbol and the CP length is longer than the channel delay spread.

Block 8 is the WiMAX receiver, whose main function is to demux the received frame and then to allocate the appropriate symbols to the corresponding user. The data symbols are retrieved by using the same permutation vectors as specified in the WiMAX transmitter *(block 4)*. These data modulated symbols are passed to either a hard-detector (binary values) or soft-detector (bit probabilities) to obtain the coded bit stream. The coded bit stream is converted to the corresponding user block size (depending on the specified system parameters) and deleaved in *block 9*. This is to ensure that the received coded bits are in the correct codeword for the channel decoder. The payload information bits are extracted from the received encoded bit stream using a Viterbi convolutional decoding algorithm [34].

After the extraction of information bits from the decoded binary stream, the values are fed to the receiver sink *(block 11)*. The function of *block 11* is to obtain the amount of errors, this is achieved by calculating the difference between the transmitted and received information sequences. These induced errors are periodically saved to result files and the sink can calculate the bit error rate (BER) for a given RF signal quality ($\frac{E_b}{N_o}$).

3.3 CONCLUSION

In this chapter, an overview of the mobile WiMAX physical layer as well as a description of the mobile WiMAX simulation platform was given. In section 3.1, the S-OFDM parameters for different bandwidths as well as the TDD frame structure was shown. The mobile WiMAX simulation platform was presented in section 3.2. The aim of this chapter is to provide a basis for the implementation of various channel estimation methods (presented in the following chapter) for mobile WiMAX.

CHAPTER FOUR

MOBILE WIMAX CHANNEL ESTIMATION

In chapter 2 it was shown that under the assumption that the guard time is longer than the channel delay spread and the CIR remains invariant within a single OFDM symbol, the received FD symbol is merely a phase rotated, amplitude scaled and noise corrupted version of the transmitted symbol. Consequently, the received symbol at an arbitrary carrier i can be expressed as

$$y_i = h_i s_i + n_i \ , \tag{4.1}$$

where y_i is the received symbol, s_i is the transmitted symbol and h_i is the channel response all in the FD. AWGN noise having a zero mean and variance of σ_n^2 is denoted as n_i. If the value of h_i is known at the receiver, single tap equalization can be performed. The zero-forcing (ZF) equalizer [35] can be expressed as

$$z_i = h_i^{-1} y_i = h_i^{-1}(h_i s_i + n_i) \ , \tag{4.2}$$

where z_i is used to infer the value of the transmitted symbol s_i. The effective noise component $\widetilde{n}_i$ in the FD can be expressed as

$$\widetilde{n}_i = h_i^{-1} n_i \ . \tag{4.3}$$

When considering the probability that a symbol A_k was transmitted, where A_k could be any one of the possible signal constellation points in the alphabet, the posterior probabilities may be expressed as follows using Bayes rule [11]

$$P(s_i = A_k | z_i) = \frac{P(z_i|s_i)P(s_i)}{P(z_i)} \ . \tag{4.4}$$

It is assumed that $\widetilde{n}_i$ is Gaussian distributed which implies that $P(z_i|s_i)$ is proportional to the Gaussian PDF

$$p(z_i|s_i) = \frac{1}{\sqrt{2\pi}\sigma_{\widetilde{n}}} e^{-\|z_i - s_i\|^2/2\sigma_{\widetilde{n}}^2} . \tag{4.5}$$

From (4.4) it is evident that $P(s_i = A_k|z_i)$ is influenced by $P(z_i|s_i)$, $P(s_i)$ and $P(z_i)$. $P(z_i)$ is the same for all symbols in the alphabet and consequently does not affect the inference of the transmitted symbol. $P(s_i)$ is not always available at the receiver and is commonly assumed to be equally probable i.e. $P(s_i) = 1/N$, where N is the number of possible symbols in the alphabet. As stated earlier, $P(z_i|s_i)$ is proportional to the PDF of the Gaussian noise as shown in (4.5). It follows that $P(s_i = A_k|z_i)$ will be maximized when the Euclidean distance $\|z_i - s_i\|^2$ is at a minimum.

In (4.2) it can be seen that perfect knowledge of h_i at the receiver is assumed when performing equalization. In practical systems, the h_i parameter is not known at the receiver and needs to be estimated. Equation 4.2 can thus be written as

$$z_i = h_{i(est)}^{-1} h_{i(act)} s_i + \widetilde{n}_i , \tag{4.6}$$

where $h_{i(est)}$ and $h_{i(act)}$ is the estimated and actual values of the CTF at carrier i respectively. The $h_{i(est)}^{-1} h_{i(act)}$ term in (4.6) causes a residual error which is governed by the relative difference between $h_{i(est)}$ and $h_{i(act)}$. It follows that the accuracy of $h_{i(est)}$ has a direct impact on detection accuracy [36].

The importance of having an accurate channel estimate can be shown graphically in Figure 4.1. In this representative example, the alphabet size is two and detection is done using the above mentioned MAP methodology. The optimal decision line is shown as x which implies that the total probability of error is proportional to the gray area. The $h_{i(est)}^{-1} h_{i(act)}$ term in (4.6) causes the decision line to be shifted to a new value x^* which causes an increase in the total probability of error area as shown by the striped area in Figure 4.1.

In this dissertation, some of the most common channel estimation methods found in the literature as well as two proposed channel estimation methods were applied to a mobile WiMAX simulation platform. This chapter is organized as follows: An overview of the two categories of pilot insertion schemes namely *block* and *comb* type pilot insertion as well as several channel estimation methods commonly associated with each of these pilot insertion schemes are given in section 4.1. In section 4.2, the pilot structure used in mobile WiMAX is presented and it is also shown how the generic OFDM estimation methods shown in section 4.1 can be applied to a mobile WiMAX system.

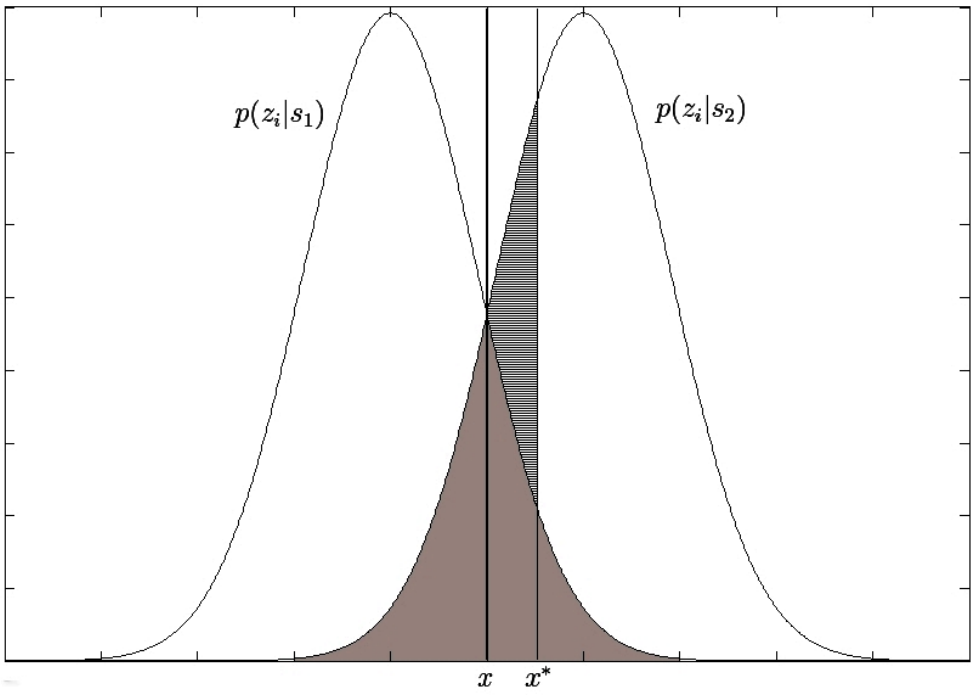

FIGURE 4.1: Graphical example of how channel estimation error influences error probability

4.1 OVERVIEW OF OFDM CHANNEL ESTIMATION

Equation (4.1) could be rewritten in matrix form as

$$\mathbf{y} = \mathbf{Sh} + \mathbf{n} \,, \tag{4.7}$$

where $\mathbf{y}$ represents the received FD symbols $[y_1 \ y_2 \ ... \ y_N]^T$, $\mathbf{S}$ is the transmitted FD sequence packed diagonally into the square matrix $\mathbf{S} = diag(s_1, s_2, ..., s_N)$, $\mathbf{h}$ is the FD channel coefficients $[h_0 \ h_1 \ ... \ h_N]^T$ and $\mathbf{n}$ is the AWGN FD noise component $[n_1 \ n_2 \ ... \ n_N]^T$.

The task at hand is to estimate $\mathbf{h}$. Symbols that are known by both the receiver and the transmitter (also known as pilot symbols) are inserted into the $\mathbf{S}$ matrix. There are two basic ways of inserting pilot symbols into a transmitted OFDM system namely *block* and *comb* type pilot insertion [37] as shown in Figure 4.2.

As could be expected, the channel estimate using a block of pilot symbols *(i.e.* $\mathbf{S}$ *matrix is fully known at the receiver)* would be much more accurate than that of comb type estimation. The problem is however that the channel would have to remain relatively constant over the series of following data

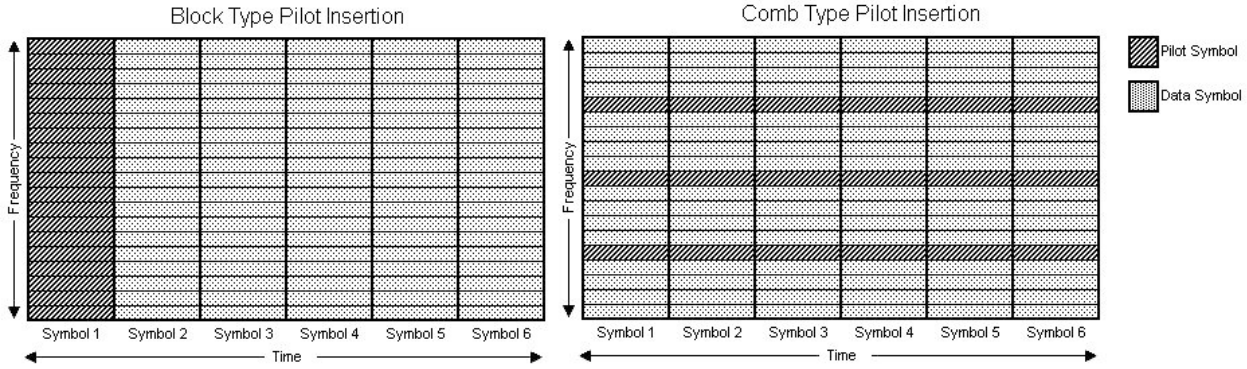

FIGURE 4.2: Comb and block type pilot insertion

blocks until the channel is re-estimated using the next block of pilot symbols. On the other hand, comb type estimation *(i.e.* $\mathbf{S}$ *matrix is only partially known at the receiver)* will give a less accurate channel prediction but the channel estimate will be updated every OFDM symbol making it more suitable for fast changing channels.

4.1.1 BLOCK TYPE CHANNEL ESTIMATION

In block type channel estimation, pilots on all subcarrier are transmitted periodically. Based on (4.7), the objective is to obtain $\mathbf{h}$ given that $\mathbf{S}$ and $\mathbf{y}$ is fully known at the receiver, with or without *a-priori* knowledge of the second order statistics of the channel. Channel estimation using the block type arrangements can be done in the TD or FD [38]. The methods evaluated in this dissertation were FD least squares (LS) [39], FD linear minimum mean square error (LMMSE) [39], FD LS using DFT improvement [40] as well as TD LS estimation [41]. A method is also proposed to expand on TD LS estimation by making use of the most significant taps (MST) approach.

4.1.1.1 FD LS ESTIMATION

The FD LS estimator is equivalent to what is referred to as the zero-forcing estimator and does not make use of second order channel statistics. Based on (4.7), LS estimation attempts to minimize the square error [42]

$$\|\epsilon\|^2 = \mathbf{n}\mathbf{n}^H = (\mathbf{y} - \mathbf{S}\mathbf{h})(\mathbf{y} - \mathbf{S}\mathbf{h})^H \,. \tag{4.8}$$

The superscript $()^H$ denotes the Hermitian transpose. The LS error can be obtained by differentiating (4.8) with respect to $\mathbf{h}$ and equating the gradient to zero as shown in (4.9)

$$\frac{\partial}{\partial \mathbf{h}}\epsilon^2 = \mathbf{2S}^H(\mathbf{y} - \mathbf{Sh}) = 0\ . \tag{4.9}$$

The solution to (4.9) equates to

$$\widehat{\mathbf{h}}_{ls} = (\mathbf{SS}^H)^{-1}\mathbf{S}^H\mathbf{y}\ . \tag{4.10}$$

It was shown in chapter 3 that if the guard time is longer than the channel delay spread and the channel is quasi-static for the duration of an OFDM burst, the $\mathbf{S}$ matrix contains only values on it's diagonal because of the absence of ISI. This implies that (4.10) can be reduced to

$$\widehat{\mathbf{h}}_{ls} = \mathbf{S^{-1}y}\ . \tag{4.11}$$

The estimation of the CTF h_i at carrier i can thus be expressed as

$$\widehat{h}_i = \frac{y_i}{s_i} = \frac{s_i h_i + n_i}{s_i}\ . \tag{4.12}$$

From (4.12) the inherent simplicity of FD LS estimation becomes evident. To obtain the CTF at a pilot carrier, the received symbol is multiplied with the inverse of the pilot value. The drawback of this method however is noise susceptibility. From (4.12), it can be seen that the noise component n_i adversely influences the performance of the estimation which results in FD LS estimation having a high mean square error (MSE) [39].

4.1.1.2 FD LMMSE ESTIMATION

By exploiting the channel correlation as well as the noise variance. The LMMSE principle can be applied to improve the $\widehat{\mathbf{h}}_{ls}$ channel estimate by multiplying $\widehat{\mathbf{h}}_{ls}$ with a weighting matrix $\mathbf{A}$ chosen to minimize the MSE

$$\min_{\mathbf{A}} E\left[\left\|\mathbf{h} - \mathbf{A}\widehat{\mathbf{h}}_{ls}\right\|^2\right]\ , \tag{4.13}$$

where $E[\,]$ denotes the expectation. The LMMSE channel estimate can thus be expressed as

$$\underbrace{\begin{bmatrix} \widehat{h}_{lmmse(1)} \\ \widehat{h}_{lmmse(2)} \\ \widehat{h}_{lmmse(3)} \\ \vdots \\ \vdots \\ \widehat{h}_{lmmse(N)} \end{bmatrix}}_{\widehat{\mathbf{h}}_{lmmse}(N\times 1)} = \underbrace{\begin{bmatrix} a_{11} & a_{12} & \dots & a_{1N} \\ a_{21} & a_{22} & \dots & a_{2N} \\ a_{31} & a_{32} & \dots & a_{3N} \\ \vdots & \vdots & \vdots & \vdots \\ \vdots & \vdots & \vdots & \vdots \\ a_{N1} & a_{N2} & \dots & a_{NN} \end{bmatrix}}_{\mathbf{A}\ (N\times N)} \underbrace{\begin{bmatrix} \widehat{h}_{ls(1)} \\ \widehat{h}_{ls(2)} \\ \widehat{h}_{ls(3)} \\ \vdots \\ \vdots \\ \widehat{h}_{ls(N)} \end{bmatrix}}_{\widehat{\mathbf{h}}_{ls}(N\times 1)}, \tag{4.14}$$

where $\widehat{h}_{lmmse(i)}$ is the LMMSE channel estimate at the i'th carrier, a_{rc} is the value of row r and column c of $\mathbf{A}$ and $\widehat{h}_{ls(i)}$ is the LS channel estimate at carrier i. When considering an arbitrary carrier i, it can be seen that the LMMSE estimate $\widehat{h}_{lmmse(i)}$ is a weighted linear combination of the LS estimate $(\widehat{\mathbf{h}}_{ls})$ over all the carriers

$$\widehat{h}_{lmmse(i)} = a_{i1}\widehat{h}_{ls(1)} + a_{i2}\widehat{h}_{ls(2)} + a_{i3}\widehat{h}_{ls(3)} + \ \dots\ + a_{iN}\widehat{h}_{ls(N)}\ . \tag{4.15}$$

The aim is to choose the weights $\mathbf{a_i} = [a_{i1}, a_{i2}, a_{i3}, ..., a_{i4}]$ to minimize the MSE which is given as

$$E\left[\left\|h_{(i)} - \left\{a_{i1}h_{ls(1)} + a_{i2}h_{ls(2)} + a_{i3}h_{ls(3)} + \ \dots\ + a_{iN}h_{ls(N)}\right\}\right\|^2\right] = E\left[\left\|\epsilon\right\|^2\right], \tag{4.16}$$

where $h_{(i)}$ represents the actual CTF at carrier i. The MSE is at a minimum when $\mathbf{a_i}$ is chosen so that the error is orthogonal to the data [42], i.e. $E\left\{\epsilon\ h_i^*\right\} = 0\ \forall\ i$. By applying the orthogonality principle, the optimal choice of $\mathbf{a_i}$ in the LMMSE sense is [42]

$$\mathbf{a_i} = \mathbf{R}^{-1}_{\widehat{\mathbf{h}}_{ls}\widehat{\mathbf{h}}_{ls}}\ \mathbf{r}\ , \tag{4.17}$$

where $\mathbf{R}_{\widehat{\mathbf{h}}_{ls}\widehat{\mathbf{h}}_{ls}} = E\{\widehat{\mathbf{h}}_{ls}\widehat{\mathbf{h}}_{ls}^H\}$ is the auto covariance of the LS estimates and $\mathbf{r}$ is the cross correlation between the LS estimates and $h_{(i)}$

$$\mathbf{r} = \begin{bmatrix} E[\widehat{h}_{ls(1)}h^*_{(i)}] \\ E[\widehat{h}_{ls(2)}h^*_{(i)}] \\ E[\widehat{h}_{ls(3)}h^*_{(i)}] \\ \vdots \\ \vdots \\ E[\widehat{h}_{ls(N)}h^*_{(i)}] \end{bmatrix}. \tag{4.18}$$

Equation (4.17) can be extended to the general form where the $\mathbf{A}$ matrix in (4.13) can be expressed as

$$\mathbf{A} = \mathbf{R}_{\mathbf{h}\widehat{\mathbf{h}}_{ls}} \mathbf{R}^{-1}_{\widehat{\mathbf{h}}_{ls}\widehat{\mathbf{h}}_{ls}} \, . \tag{4.19}$$

It is shown in [43] that (4.19) can be written as

$$\widehat{\mathbf{h}}_{lmmse} = \mathbf{A}\widehat{\mathbf{h}}_{ls} = \mathbf{R}_{\mathbf{hh}}(\mathbf{R}_{\mathbf{hh}} + \sigma_n^2(\mathbf{SS^H})^{-1})^{-1}\widehat{\mathbf{h}}_{ls} \, , \tag{4.20}$$

where $\mathbf{R}_{\mathbf{hh}} = E\{\mathbf{h}\mathbf{h}^H\}$ is the channel autocorrelation matrix with σ_n^2 being the noise variance. From (4.20) it can be observed that by exploiting the channel autocorrelation and noise variance, the accuracy of the FD LS estimate ($\widehat{\mathbf{h}}_{ls}$) calculated in (4.12) can be increased. In [39] it was shown that LMMSE has an improvement of between 10 and 15 dB over LS estimation when considering the MSE. The disadvantage of LMMSE is the complexity as well as the need for second order channel statistics which is not always available in practical systems.

4.1.1.3 FD LS ESTIMATION WITH DFT IMPROVEMENT

In this method, the LS estimate obtained in (4.11) is improved by exploiting the fact that the number of CIR taps are usually far less than the FFT size, i.e. $L + 1 << N$. The TD transformation of the LS estimate $\widehat{\mathbf{h}}_{\mathbf{ls}}$ yields

$$\widehat{\mathbf{c}} = \mathbf{F}_{\mathbf{N}}^{-\mathbf{1}}\widehat{\mathbf{h}}_{\mathbf{ls}} \, . \tag{4.21}$$

Figure 4.3 gives an example of a CIR estimate obtained using (4.21) under various SNR conditions. In this example an FFT size of 128 was used with a CIR where only the first 6 taps contain actual signal energy. As seen in Figure 4.3, the noise component in the FD LS estimate constitutes to an error over all the taps of the CIR. It can be seen that as $\frac{E_b}{N_o}$ increases, the noise on the zero energy taps of the CIR (i.e. taps 7 to 128) decreases.

As stated previously, the CIR only has a finite number of taps which is usually much less than the FFT size, the "high frequency" region can thus be set to zero as shown in [40] where

$$\widehat{c}(p) = \begin{cases} \widehat{c}(p), & 0 \leq p \leq p_c \\ 0, & otherwise \end{cases} \, . \tag{4.22}$$

Because it is assumed that the channel delay spread does not exceed the CP length, the value of p_c in (4.22) is usually set to the CP size. Various methods attempt to estimate the length of the MST to further improve estimation [40, 44, 45].

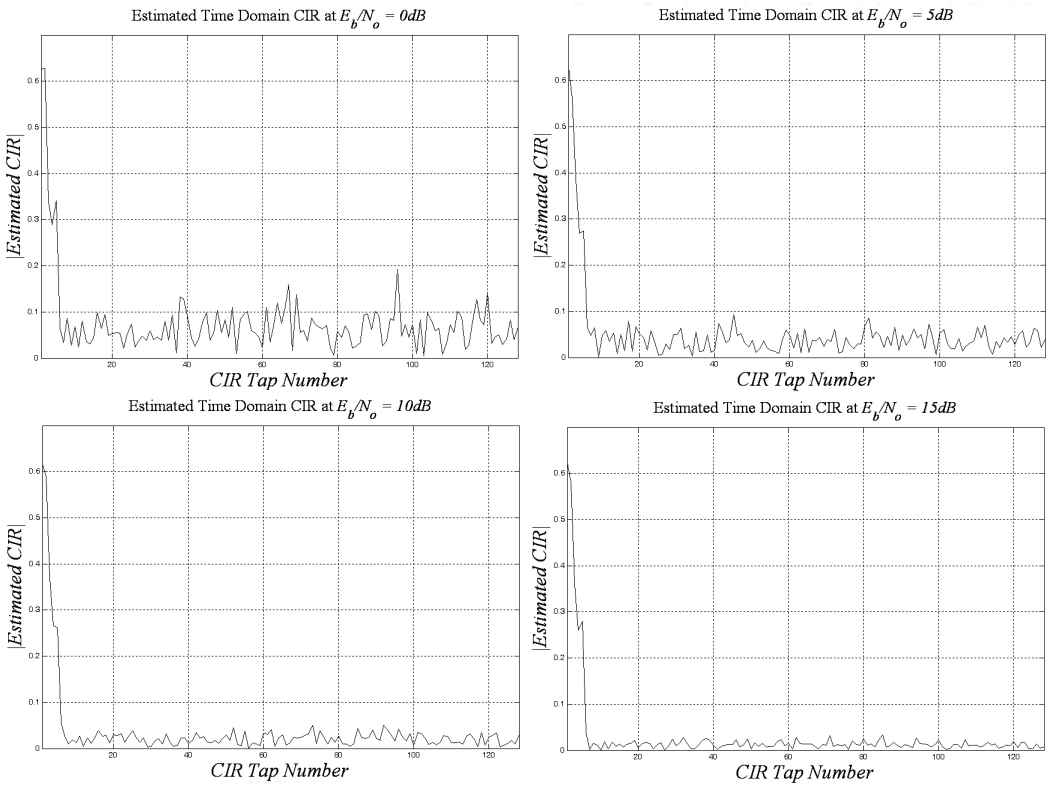

FIGURE 4.3: Estimated CIR under various SNR conditions

4.1.1.4 TD LS ESTIMATION

Conforming to the OFDM model presented in chapter 2, the TD vector $\mathbf{r}$ at the receiver after CP removal can be expressed as

$$\underbrace{\begin{bmatrix} r_1 \\ r_2 \\ r_3 \\ \vdots \\ \vdots \\ r_N \end{bmatrix}}_{N\times 1} = \underbrace{\begin{bmatrix} x_1 & x_N & x_{N-1} & \dots & x_{N-L+1} \\ x_2 & x_1 & x_N & \dots & x_{N-L} \\ x_3 & x_2 & x_1 & \dots & x_{N-L-1} \\ \vdots & \vdots & \vdots & \vdots & \vdots \\ \vdots & \vdots & \vdots & \vdots & \vdots \\ x_N & x_{N-1} & x_{N-2} & \dots & x_{N-L} \end{bmatrix}}_{N\times L+1} \underbrace{\begin{bmatrix} c_0 \\ c_1 \\ c_2 \\ \vdots \\ \vdots \\ c_L \end{bmatrix}}_{L+1\times 1} + \underbrace{\begin{bmatrix} n_1 \\ n_2 \\ n_3 \\ \vdots \\ \vdots \\ n_N \end{bmatrix}}_{N\times 1}, \tag{4.23}$$

where $[c_0\ c_1\ ...\ c_L]$ is the CIR of length $L+1$, x_i is the i'th TD symbol and n_i is AWGN noise. Equation (4.23) can be written in matrix notation as

$$\mathbf{r} = \mathbf{X}\mathbf{c} + \mathbf{n}\,. \tag{4.24}$$

Because a block type pilot structure is used, it is assumed that $\mathbf{X}$ is known *a-priori* at the receiver. An estimate of the channel $\widehat{\mathbf{c}}$ can be made by using the method of LS. Using the same methodology as in

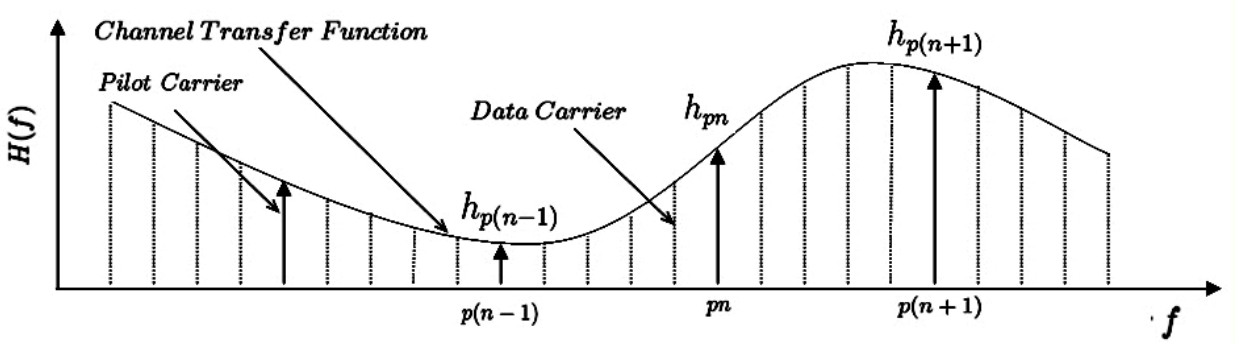

FIGURE 4.4: Pilot carrier index example

FD LS estimation (section 4.1.1.1), the estimated channel $\widehat{\mathbf{c}}$ can be written as

$$\widehat{\mathbf{c}} = (\mathbf{X}^{\mathbf{H}}\mathbf{X})^{-1}\mathbf{X}^{\mathbf{H}}\mathbf{r}\,. \tag{4.25}$$

The LS estimate shown in (4.25) always has a solution [42]. It is therefore important to determine whether the solution to (4.25) is unique. This requirement is covered by the uniqueness theorem in [46] which states that a unique solution to the LS problem can only be expected when the $\mathbf{X}$ matrix in (4.25) has linearly independent columns. This implies that the system of equations should be overdetermined, i.e. more equations than unknowns [42]. In (4.23) it can be seen that the dimension of $\mathbf{X}$ is $N \times L+1$ where $N >> L+1$. This implies that the system in (4.25) will always be overdetermined. The only prerequisite for $\widehat{\mathbf{c}}$ to be unique is that the columns of $\mathbf{X}$ should be independent.

Another important point to consider is that the number of taps of the actual CIR $(L+1)$ is not known at the receiver. The number of estimated taps is usually set to the CP length because the assumption is that the CP length is longer than the channel delay spread. If the number of MST are known at the receiver, an improved estimate can be made of the CIR. In section 4.2.2.4, a method is proposed to determine the number of MST.

4.1.2 COMB TYPE CHANNEL ESTIMATION

With comb type channel estimation, pilot symbols are inserted in the data sequence to allow for channel estimation [43, 47, 48]. From Figure 4.4 it can be seen that the aim is to infer the CFT over the entire OFDM symbol given a series of channel estimates at pilot positions. There are numerous methods of inferring the CTF using pilot tones multiplexed with data tones. A popular time domain method is frequency pilot time average (FPTA) where positive and negative alternatively polarized pilot tones are multiplexed with data symbols [49]. Other methods extend on the methodology used

in section 4.1.1.3 to the interpolation case [40]. Because of the of the non-uniform pilot structure and pseudo random polarization scheme used in FUSC mobile WiMAX [9] (discussed in more detail in section 4.2.1), only FD interpolation based methods were considered in the case of comb type channel estimation for mobile WiMAX. Interpolation based methods determine the CTF of the entire symbol by estimating the CTF at the pilot carriers and then interpolating between these estimates to obtain an estimate over the entire OFDM symbol. The interpolation methods considered in this dissertation were piecewise constant (PC), linear, spline cubic and Wiener interpolation. An adaptive FD LS interpolation method is also proposed in section 4.1.2.5

As shown in section (4.1.1.1), an estimate of the CTF at an arbitrary pilot tone can be calculated in the LS sense as

$$\widehat{h}_{pn} = \frac{y_{pn}}{s_{pn}} \quad n = 1, .., M \ , \tag{4.26}$$

where h_{pn} is the channel estimate at the n'th pilot carrier and M is the total number of pilot symbols. The carrier index of the n'th pilot is based on the specific pilot insertion scheme.

4.1.2.1 PIECEWISE CONSTANT INTERPOLATION

In the case of PC interpolation, a channel estimate is obtained from pilot pn $(\widehat{h}_{pn})$ and is then constantly interpolated at the data carriers in the set F defined as [50]

$$F = f : f \in \left[\frac{(pn + p(n-1))}{2}, \frac{(pn + p(n+1))}{2} \right] \ . \tag{4.27}$$

Figure 4.5 gives a representative example of PC interpolation. As can be seen from this example, even if the channel could be perfectly estimated at the pilot positions, there is still a significant difference between the PC approximated CTF and the actual CTF. This error is commonly referred to as a systematic error and is shown graphically by the filled area.

4.1.2.2 LINEAR INTERPOLATION

Linear interpolation is done using the following equation [50]

$$\widehat{h}_{di} = \frac{\widehat{h}_{p(n+1)} - \widehat{h}_{pn}}{p(n+1) - pn}.(di - pn) + \widehat{h}_{pn} \ , \tag{4.28}$$

where $pn < di < p(n+1)$, pn and di is the carrier index for the n'th pilot and i'th data tone respectively. An example of linear interpolation can be seen in Figure 4.6. As with PC interpolation, there exists a systematic error in the estimated linear CTF. In this example it can be seen that the

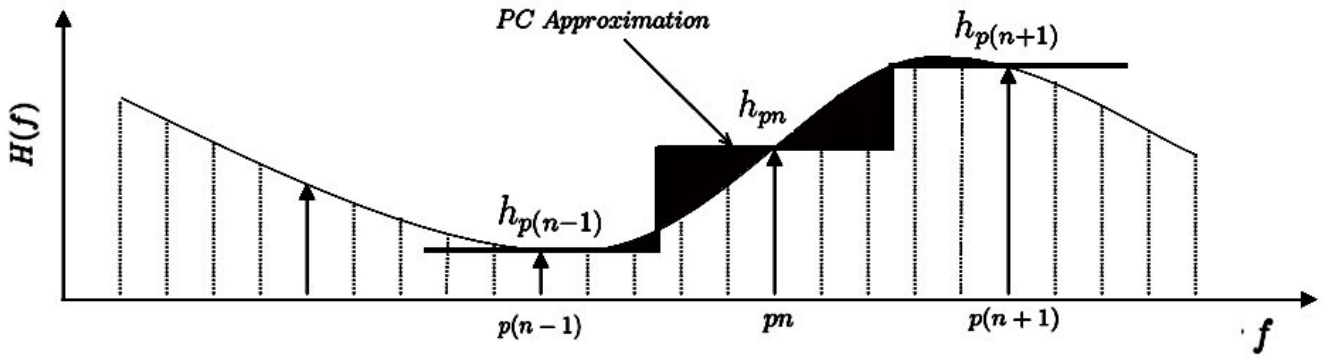

FIGURE 4.5: Piecewise constant interpolation

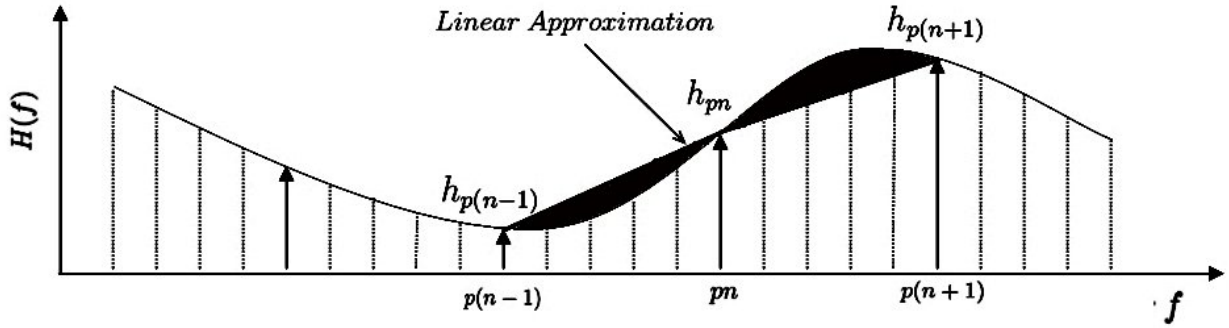

FIGURE 4.6: Linear interpolation

systematic error appears less than that of PC interpolation. This observation is confirmed in [50] where it was shown that linear interpolation significantly outperforms PC interpolation when considering channel estimation of an arbitrary CTF.

4.1.2.3 SPLINE CUBIC INTERPOLATION

Spline cubic interpolation was done using equations 4.29, 4.30, 4.31 and 4.32

$$A = \frac{z_{i+1}(di - pn)^3 + z_i(p(n+1) - di)^3}{6k_n} \tag{4.29}$$

$$B = \left(\frac{h_{p(n+1)}}{k_n} - \frac{k_n z_n}{6}\right)(di - pn) \tag{4.30}$$

$$C = \left(\frac{h_{pn}}{k_n} - \frac{k_n z_n}{6}\right)(p(n+1) - di) \tag{4.31}$$

$$h_{di} = A + B + C \tag{4.32}$$

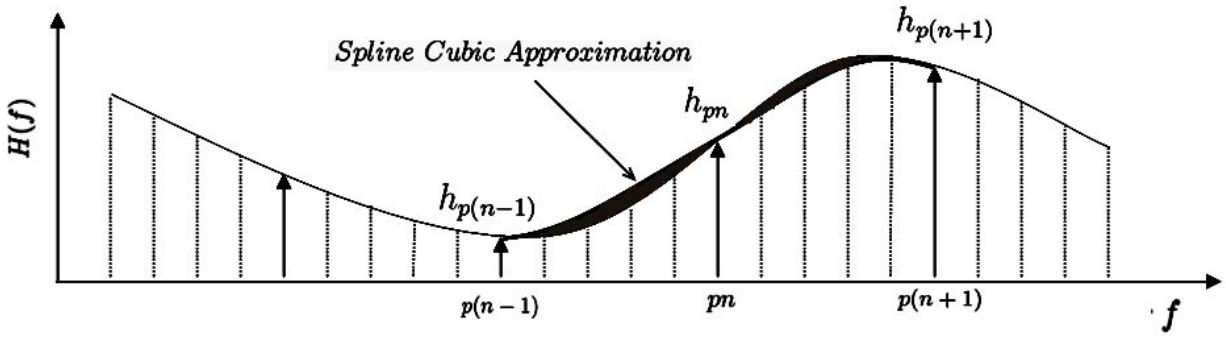

FIGURE 4.7: Spline cubic interpolation

The data carrier index di lies between two pilots with carrier index $p(n)$ and $p(n+1)$ respectively. In (4.29), (4.30) and (4.31), $k_n = p(n+1) - p(n)$ and $n = 1, 2, .., M-1$ with M being the total number of pilot tones. The coefficients z_n can be obtained by setting $D_1 = D_2$ and solving

$$D_1 = k_{n-1}z_{n-1} + 2(k_{n-1} + k_n)z_n + k_n z_{n+1}$$

$$D_2 = 6\left(\frac{h_{p(n+1)} - h_{pn}}{k_n} - \frac{h_{pn} - h_{p(n-1)}}{k_{n-1}}\right)$$

An example of spline cubic interpolation is shown in Figure 4.7 where is can visually be seen that a smooth and continuous polynomial is fitted to the given data points. When visually compared to PC and linear interpolation, it can be observed that the systematic error is not as severe. This observation is confirmed in [37] where it was shown that the systematic error produced using spline cubic interpolation for comb type channel estimation is less than that of PC as well as linear interpolation.

4.1.2.4 DISCRETE WIENER INTERPOLATION

When considering Figure 4.4, it is intuitive that there exists a correlation between the channel coefficients at the pilot and data carriers. Using a linear combination of the CTF at the pilot tones, a channel estimate at the data tones can be obtained. Figure 4.8 shows the structure of this linear filter. Here, m is the total number of pilot symbols, $\widehat{h}_{di}$ is the estimated CTF at data tone i and $\widehat{h}_{pm}$ is the estimated CTF at pilot tone m. The tap weight $w_{q(di)}$ is the q'th weight used for calculating $\widehat{h}_{di}$. It can be seen that $\widehat{h}_{di}$ is a weighted linear combination of the channel coefficients estimated at the pilot carriers ($\widehat{h}_{p1}$ $\widehat{h}_{p2}$ ... $\widehat{h}_{pm}$).

To obtain the optimum tap-weights in the LMMSE sense, the orthogonality principle *(see section 4.1.1.2)* can be used. Using the same methodology as in section 4.1.1.2, the optimal weight coefficients

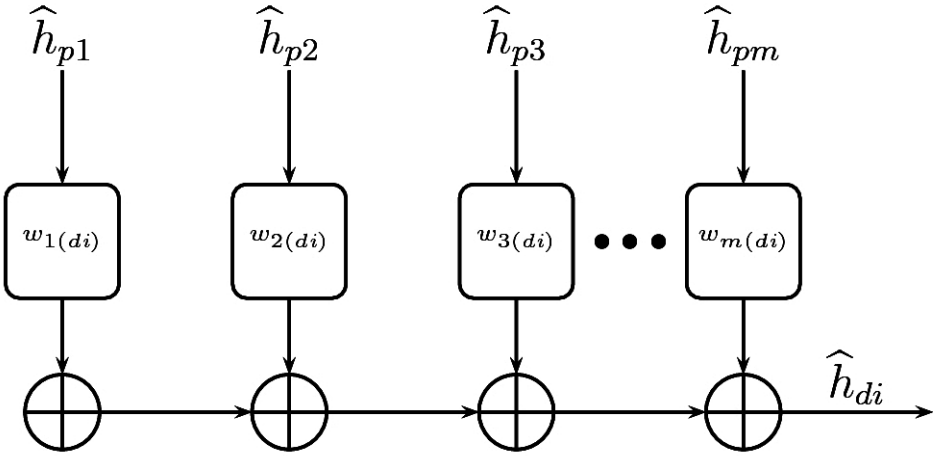

FIGURE 4.8: Linear filter

can be calculated as

$$\mathbf{w}_{di} = \mathbf{R}_{\mathbf{hh}}^{-\mathbf{1}}\mathbf{r} \, , \tag{4.33}$$

where $\mathbf{w}_{di}$ is a vector containing the weights associated with each pilot estimate $[w_{1(di)}\ w_{2(di)}\ ...\ w_{m(di)}]$, $\mathbf{R_{hh}}$ is the channel autocorrelation matrix and $\mathbf{r}$ is the cross-correlation vector between the data carrier h_{di} and pilot carriers $[h_{p1}\ h_{p2}\ ...\ h_{pm}]$. Equation (4.33) can be used to calculate the weights for all the data carriers. The estimated CTF is consequently calculated as

$$\widehat{\mathbf{h}}_d = \mathbf{A}\widehat{\mathbf{h}}_p \, , \tag{4.34}$$

where $\widehat{\mathbf{h}}_d = [\widehat{h}_{d1}\ \widehat{h}_{d2}\ ...\ \widehat{h}_{dd}]^T$ and $\widehat{\mathbf{h}}_p = [\widehat{h}_{p1}\ \widehat{h}_{p2}\ ...\ \widehat{h}_{pm}]^T$. It is assumed that there are d data and m pilot carriers. $\mathbf{A}$ is the weighting matrix in the following form

$$\mathbf{A} = \begin{bmatrix} w_{1(d1)} & w_{2(d1)} & \dots & w_{m(d1)} \\ w_{1(d2)} & w_{2(d2)} & \dots & w_{m(d2)} \\ w_{1(d3)} & w_{2(d3)} & \dots & w_{m(d3)} \\ \vdots & \vdots & \vdots & \vdots \\ \vdots & \vdots & \vdots & \vdots \\ w_{1(dd)} & w_{2(dd)} & \dots & w_{m(dd)} \end{bmatrix} . \tag{4.35}$$

Discrete Wiener interpolation is optimal in the MSE sense and has the advantage that the symbols can be arbitrarily spaced. The disadvantage of this method is that the channel autocorrelation needs to be

known *a-priori* at the receiver, in a mobile environment where the CIR is continually changing, this is not always possible.

4.1.2.5 ADAPTIVE LS INTERPOLATION

In this section, a method is proposed to extend on the discreet Wiener interpolation method presented in the previous section. As shown in the previous section, the second order channel statistics are needed to determine the optimal weighting matrix $\mathbf{A}$ in (4.35). These second order statistics are however not always available in practice. An adaptive LS interpolation algorithm is proposed in this section which does not require any *a-priori* knowledge at the receiver. The methodology of determining the CTF over the data carriers is exactly the same as in (4.34), the difference however is in the calculation of the $\mathbf{A}$ matrix. Using the method of LS, the $\mathbf{A}$ matrix can be determined in a deterministic fashion by making use of prior symbol observations.

If N training symbols that are fully known by both the transmitter and receiver are transmitted, the value of both $\widehat{\mathbf{h}}_p$ and $\widehat{\mathbf{h}}_d$ in (4.34) can be determined by means of FD LS estimation as shown in section 4.1.1.1. When considering the estimated CTF at data carrier i , there are N independent observations of both $\widehat{h}_{di}$ and $\widehat{\mathbf{h}}_p$. It follows that for each symbol, the estimated value of the CTF at data carrier di ($\widehat{h}_{di}$) can be written as a weighted linear combination of all the pilot CTF estimates $\widehat{\mathbf{h}}_p$ as

$$\underbrace{\begin{bmatrix} \widehat{h}_{p1(1)} & \widehat{h}_{p2(1)} & \dots & \widehat{h}_{pm(1)} \\ \widehat{h}_{p1(2)} & \widehat{h}_{p2(2)} & \dots & \widehat{h}_{pm(2)} \\ \widehat{h}_{p1(3)} & \widehat{h}_{p2(3)} & \dots & \widehat{h}_{pm(3)} \\ \vdots & \vdots & \vdots & \vdots \\ \vdots & \vdots & \vdots & \vdots \\ \widehat{h}_{p1(N)} & \widehat{h}_{p2(N)} & \dots & \widehat{h}_{pm(N)} \end{bmatrix}}_{\mathbf{H}_p(N\times m)} \underbrace{\begin{bmatrix} w_{1(di)} \\ w_{2(di)} \\ w_{3(di)} \\ \vdots \\ \vdots \\ w_{m(di)} \end{bmatrix}}_{\mathbf{w}_{di}\ (m\times 1)} = \underbrace{\begin{bmatrix} \widehat{h}_{di(1)} \\ \widehat{h}_{di(2)} \\ \widehat{h}_{di(3)} \\ \vdots \\ \vdots \\ \widehat{h}_{di(N)} \end{bmatrix}}_{\mathbf{h}_{di}\ (N\times 1)}, \tag{4.36}$$

where $\widehat{h}_{pa(b)}$ is the channel estimate at the a'th pilot of symbol b and $\widehat{h}_{di(b)}$ is the channel estimate at the i'th data carrier of symbol b. The task at hand is thus to determine $\mathbf{w}_{di}$ given N fully known OFDM symbols.

Writing (4.36) in vector notation

$$\mathbf{H}_p\mathbf{w}_{di} = \mathbf{h}_{di}\ . \tag{4.37}$$

The LS estimate of $\mathbf{w}_{di}$ is

$$\mathbf{w}_{di} = (\mathbf{H}_p^H \mathbf{H}_p)^{-1} \mathbf{H}_p^H \mathbf{h}_{di} \ . \tag{4.38}$$

By using 4.38, the weighting coefficients $[\mathbf{w}_{d1}\ \mathbf{w}_{d2}\ ...\ \mathbf{w}_{dd}]$ can be calculated. Having $\mathbf{A} = [\mathbf{w}_{d1}^T\ \mathbf{w}_{d2}^T\ ...\ \mathbf{w}_{dd}^T]$, equation (4.34) can be used to find the CTF for all the data carriers. The advantage of the proposed method is that no *a-priori* knowledge of the channel autocorrelation is needed. A possible disadvantage is that when the mobile environment changes rapidly, the weights would have to be recalculated frequently. Another important aspect is the number of OFDM symbols that are required to effectively train the **A** matrix. The implication of which will be discussed in more detail in section 4.2.3.4

4.2 APPLYING THE CHANNEL ESTIMATION METHODS TO A MOBILE WIMAX SYSTEM

In the previous section, a number of channel estimation methods based on both comb and block type channel estimation were discussed and analyzed. In this section, the pilot structure used in mobile WiMAX will be shown followed by a description on how each of the channel estimation methods presented in the previous sections can be applied to the mobile WiMAX physical layer discussed in chapter 3.

4.2.1 MOBILE WIMAX PILOT STRUCTURE

The frame structure for mobile WiMAX was shown in Figure 3.2 where it can be seen that each frame consists of an initial preamble followed by a series of data symbols. The preamble contains only pilot carriers, guard bands and a DC carrier whereas data symbols consists of pilot carriers, data carriers, guard bands as well as a DC carrier. When considering data symbols, there exits two types of pilot sets namely *variable* and *fixed* [9, 17]. As their name suggests, in a fixed pilot set, pilot positions are the same for any given symbol whereas a variable pilot set differs for each symbol. When considering the variable pilot set, the pilot positions are calculated as follows

$$PilotsLocation = VariableSet\ +\ 6(SymbolNumber\ \mathbf{mod}\ 2) \ . \tag{4.39}$$

From (4.39), it can be seen that the pilot locations are offset by 6 carriers for even and odd symbols. An example of the pilot structure for mobile WiMAX operating in FUSC mode using 128-FFT is shown in Figure 4.9 where the pilot locations for the preamble as well as odd and even data symbols are shown.

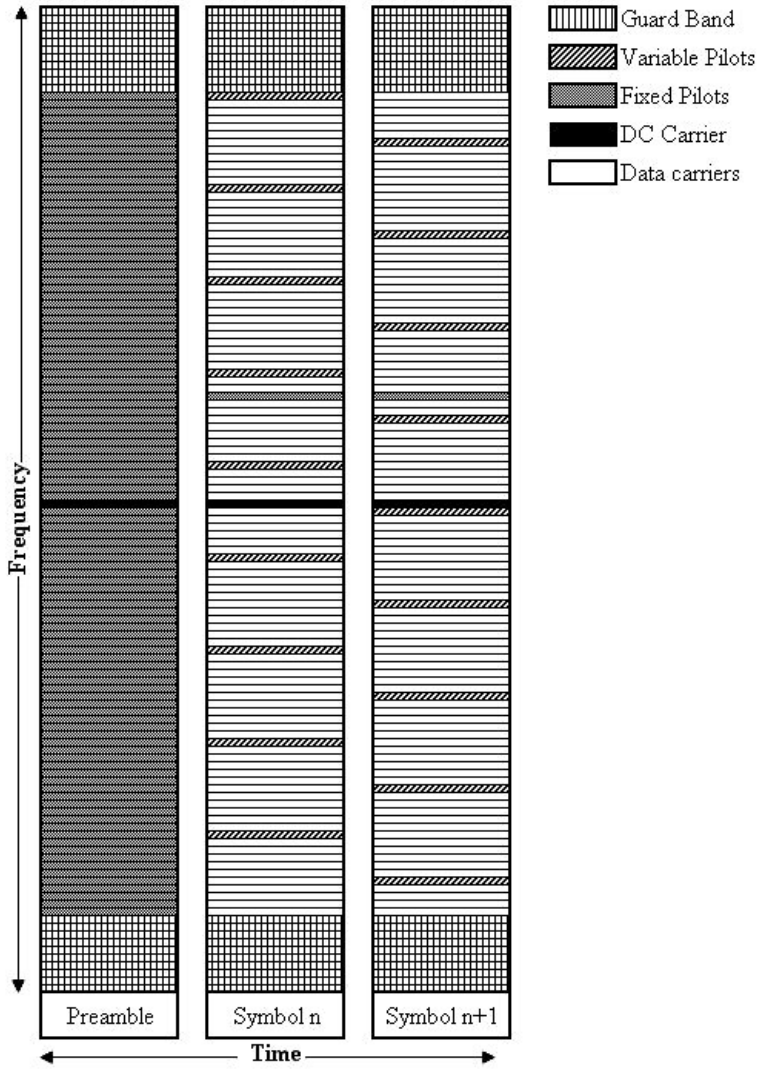

FIGURE 4.9: Mobile WiMAX 128-FFT pilot structure

In the previous section, channel estimation methods based on block and comb type pilot arrangements were discussed. When considering the mobile WiMAX pilot structure, the preamble can be regarded as a block type arrangement because the entire symbol in known by both the transmitter and receiver. The pilot structure used in data symbols can be considered as a "special" case of comb type pilot insertion where pilot positions are offset for even and odd symbols. Because the pilot arrangement is not quite that of the classical comb type pilot arrangement, the broader classification of pilot symbol assisted modulation (PSAM) will be used when referring to the "special" form of comb type pilot arrangement used in mobile WiMAX. The estimation methods presented in the previous section that were based on the block type pilot arrangement can be directly applied on the preamble used in mobile WiMAX while the channel estimation methods based on the classical comb type pilot arrangements will be applied to the PSAM arrangement used in mobile WiMAX.

4.2.2 PREAMBLE CHANNEL ESTIMATION

This section will discuss how the block type channel estimation methods given in section 4.1.1 can be applied to a mobile WiMAX system where the use of guard bands and the DC carrier requires some modifications to be made to these generic methods.

4.2.2.1 FD LS ESTIMATION

In section 4.1.1.1 it was shown that the CTF at carrier i can be calculated as

$$\widehat{h}_i = \frac{y_i}{s_i} \;\; i = 1, .., N \;, \tag{4.40}$$

where $\widehat{h}_i$ is the estimated CTF, y_i is the received symbol and s_i the transmitted symbol at carrier i. As shown in Figure 4.9, the preamble contains left and right guard bands as well as a DC carrier. Assuming N_l and N_r is the value of the first and last information bearing tone index respectively and N_{dc} is the index of the DC carrier pilot tone, (4.40) can then be written as

$$\widehat{h}_i = \frac{y_i}{s_i} \;\; i = N_l, .., N_r \;\; i \neq N_{dc} \;. \tag{4.41}$$

4.2.2.2 FD LMMSE ESTIMATION

In section 4.1.1.2 it was shown that the LMMSE channel estimate can be written as

$$\widehat{\mathbf{h}}_{lmmse} = \mathbf{R_{hh}}(\mathbf{R_{hh}} + \sigma_n^2(\mathbf{SS^H})^{-1})^{-1}\widehat{\mathbf{h}}_{ls} \;, \tag{4.42}$$

where $\mathbf{R_{hh}} = E\{\mathbf{hh}^H\}$ is the channel autocorrelation matrix with σ_n^2 being the noise variance. The LS estimate $\widehat{\mathbf{h}}_{ls}$ is calculated using (4.41) and $\mathbf{S}$ is a diagonal matrix with $\mathbf{S} = diag(s_1, s_2, s_3, ..., s_N)$. Applying the algorithm to a mobile WiMAX system, the $(\mathbf{SS^H})^{-1}$ term in (4.42) is replaced with its expectation [43] $E\{(\mathbf{SS^H})^{-1}\}$ = $E\{\|\frac{1}{s_k}\|^2\}\mathbf{I}$. The modulation scheme used on the pilot carriers of the preamble is BPSK [9]. This implies that the value of $E\{\|\frac{1}{s_k}\|^2\} = 1$ because $s_k = \pm 1$. It follows that (4.42) can be reduced to

$$\widehat{\mathbf{h}}_{lmmse} = \mathbf{R_{hh}}(\mathbf{R_{hh}} + \sigma_n^2\mathbf{I})\widehat{\mathbf{h}}_{ls} \;. \tag{4.43}$$

It is important to note that the noise variance σ_n^2 is in the FD. It was proved in [44] that the relation between the noise variance in the FD and TD is

$$\sigma_f^2 = N\sigma_t^2 \;, \tag{4.44}$$

where σ_f^2 and σ_t^2 is the noise variance in the FD and TD respectively and N is the FFT size.

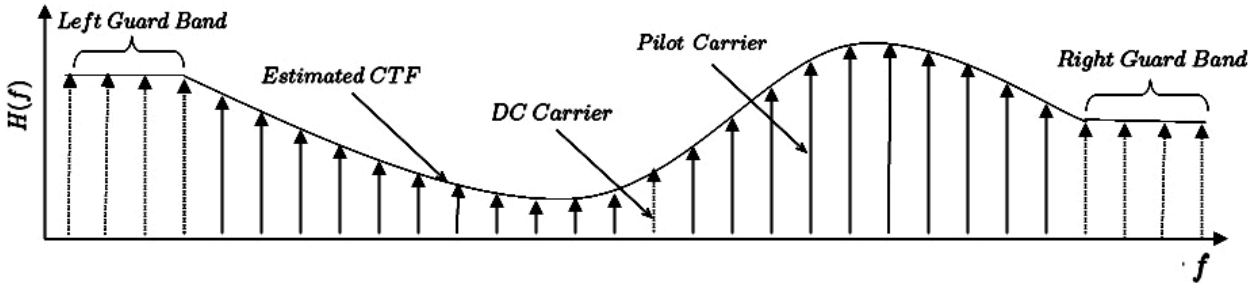

FIGURE 4.10: Adapting the FD LS with DFT improvement to mobile WiMAX

4.2.2.3 FD LS ESTIMATION WITH DFT IMPROVEMENT

As shown in section 4.1.1.3, the FD LS estimated CTF can be improved by transforming into the TD and setting the CIR taps believed to have no energy to zero. The filtered CIR is then transformed back into the FD. From (4.41) it is evident that because of the guard bands and DC carrier, $\widehat{\mathbf{h}}_{ls}$ is not fully known. This will affect $\widehat{\mathbf{c}}$ because of the convolutional nature of the IDFT transformation. To apply this method to a WiMAX system, the values of $\widehat{\mathbf{h}}_{ls}$ at the guard bands and DC carrier needs to be estimated. This was done using PC interpolation on the guard bands and linear interpolation for the DC carrier as shown in Figure 4.10.

4.2.2.4 TD LS ESTIMATION

As shown in section 4.1.1.4, the CIR can be calculated as follows

$$\widehat{\mathbf{c}} = (\mathbf{X^H X})^{-1}\mathbf{X^H r}\,, \tag{4.45}$$

where $\widehat{\mathbf{c}}$ is the estimated CIR, $\mathbf{X}$ is a matrix containing the values of the transmitted TD vector $[x_1\ x_2\ x_3\ ...\ x_N]$ and $\mathbf{r}$ is the received TD vector. When applying the TD LS method to a mobile WiMAX system, $\mathbf{r}$ is the TD OFDMA symbol after CP removal and $[x_1 x_2 x_3 ... x_N]$ is merely the OFDMA symbol after the IDFT operation at the receiver. Because the preamble is known at the receiver, the IDFT operation can be used to determine the TD transform of the preamble. It follows that the $(\mathbf{X^H X})^{-1}\mathbf{X^H}$ part of (4.45) can easily be precomputed and stored at the receiver. From (4.23) it can be seen however that $\mathbf{X}$ is of dimension $N \times L+1$. This implies that in the construction of the $\mathbf{X}$ matrix, the number of estimated taps need to be considered.

A common method is to set the estimated taps to the CP length because it is inherently assumed that the system design is such that the CIR length is shorter than the CP length *(see chapter 2)*. The problem with this method is that if the CIR length is much shorter than the CP length (which is often

Step	Comment
1	Obtain TD received vector $\rightarrow \mathbf{r}_{cp}$
2	Remove CP $\rightarrow \mathbf{r}$
3	Calculate LS estimate using the CP length $\rightarrow \widehat{\mathbf{c}}_{cp} = (\mathbf{X}_{cp}^H \mathbf{X}_{cp})^{-1} \mathbf{X}_{cp}^H \mathbf{r}$
4	Obtain the MST
5	Calculate LS estimate using the MST length $\rightarrow \widehat{\mathbf{c}}_{mst} = (\mathbf{X}_{mst}^H \mathbf{X}_{mst})^{-1} \mathbf{X}_{mst}^H \mathbf{r}$

TABLE 4.1: MST LS algorithm

the case [44, 45]), the accuracy of the estimated CIR is adversely affected.

In this dissertation, a two stage TD LS estimation approach is proposed to improve on CP length assumption. Table 4.1 gives an overview of the algorithm that was used. An initial TD LS estimation is done by setting the number of taps to be estimated equal to the CP length *(step 3)* were $\mathbf{X}_{cp}$ is constructed as

$$\mathbf{X}_{cp} = \underbrace{\begin{bmatrix} x_1 & x_N & x_{N-1} & \dots & x_{N-CP+2} \\ x_2 & x_1 & x_N & \dots & x_{N-CP+3} \\ x_3 & x_2 & x_1 & \dots & x_{N-CP+4} \\ \vdots & \vdots & \vdots & \vdots & \vdots \\ x_{CP} & x_{CP-1} & x_{CP-2} & \dots & x_1 \\ \vdots & \vdots & \vdots & \vdots & \vdots \\ x_N & x_{N-1} & x_{N-2} & \dots & x_{N-CP+1} \end{bmatrix}}_{N \times CP}, \tag{4.46}$$

and $\mathbf{X}_{mst}$ is constructed as

$$\mathbf{X}_{mst} = \underbrace{\begin{bmatrix} x_1 & x_N & x_{N-1} & \dots & x_{N-MST+2} \\ x_2 & x_1 & x_N & \dots & x_{N-MST+3} \\ x_3 & x_2 & x_1 & \dots & x_{N-MST+4} \\ \vdots & \vdots & \vdots & \vdots & \vdots \\ x_{MST} & x_{MST-1} & x_{MST-2} & \dots & x_1 \\ \vdots & \vdots & \vdots & \vdots & \vdots \\ x_N & x_{N-1} & x_{N-2} & \dots & x_{N-MST+1} \end{bmatrix}}_{N \times MST}. \tag{4.47}$$

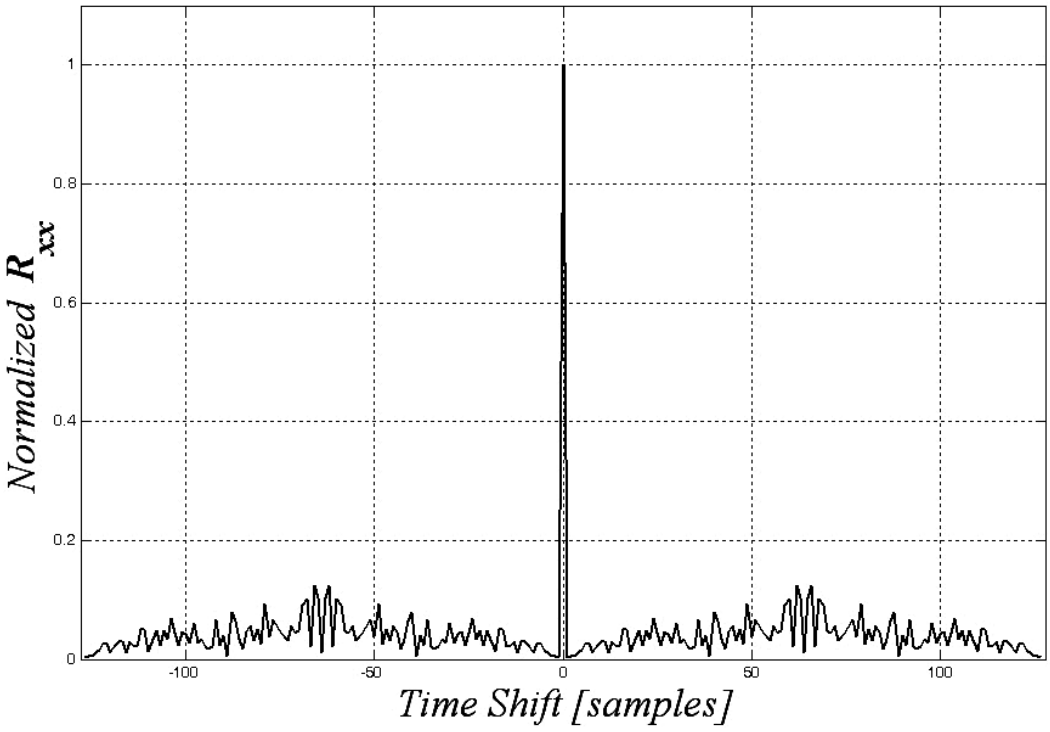

FIGURE 4.11: Normalized autocorrelation of a TD preamble symbol

In (4.46) and (4.47), CP is the CP length and MST is the MST length respectively. After the initial LS estimate based on the CP length is made, the number of MST are selected *(step 4)*. This is done by using the maximum excess delay. The maximum excess delay is defined to be the delay during which the multipath energy falls within X dB below the maximum [1]. The value of X for this application was chosen as 10 dB. After the number of MST are obtained, the LS estimate is once again done but this time using $\mathbf{X}_{mst}$ *(step 5)*. The performance of the proposed MST LS method is shown in chapter 5.

In section 4.1.1.4 it was mentioned that for the LS estimate to have a unique solution, the columns of the $\mathbf{X}$ matrix in (4.45) need to be independent. For this reason a pseudo noise (PN) sequence is used in mobile WiMAX to generate the preamble [9]. Figure 4.11 shows the normalized autocorrelation of a TD preamble symbol generated according to the 802.16e-2005 standard. It can be seen that autocorrelation of the preamble approximates a Kronecker delta function which implies that time shifted versions of the preamble are linearly independent.

4.2.3 PSAM CHANNEL ESTIMATION

This section will explain how the comb type channel estimation methods described in section 4.1.2 was applied to mobile WiMAX. As was shown in Figure 4.9, the data symbols contain pilot symbols,

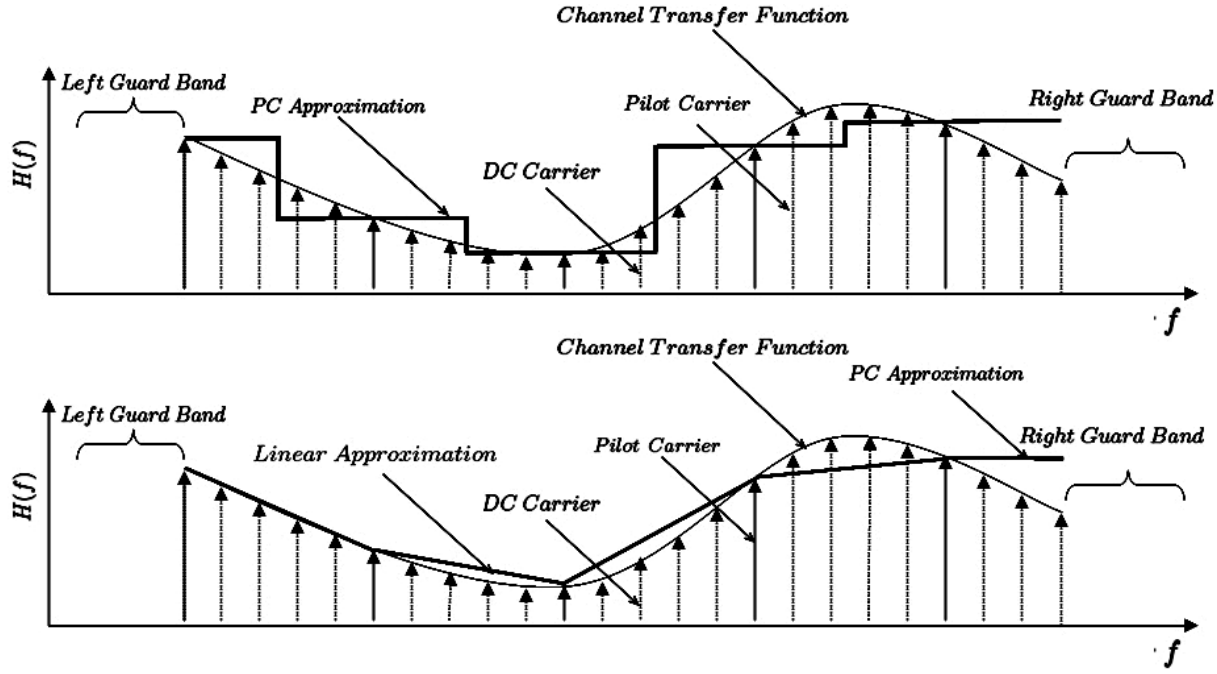

FIGURE 4.12: Adapting PC and linear interpolation for mobile WiMAX

data symbols, guard bands as well as a DC carrier.

4.2.3.1 PC AND LINEAR INTERPOLATION

PC and linear interpolation can be directly applied to mobile WiMAX as shown in Figure 4.12. From this representation it is shown that the interpolation is not extended to the guard bands because only the CTF estimates at the data carriers are used for equalization. Figure 4.9 shows that that the pilot carriers are not always located on the first and last information bearing carrier. This does not influence the PC interpolation scheme but does influence linear interpolation. From the example in Figure 4.12, it can be seen that the right most carrier is not a pilot tone. It follows that the CTF at the right edge needs to be calculated by means of extrapolation rather than interpolation. In this dissertation, a PC method was used to calculate the CTF at these edges as shown in Figure 4.12.

4.2.3.2 SPLINE CUBIC INTERPOLATION

The spline cubic interpolator discussed in section 4.1.2.3 can be directly used in a mobile WiMAX system. As with linear interpolation, in the case where pilot carriers were not available at the edges of the symbol, the CTF at data carriers were approximated using PC interpolation.

4.2.3.3 DISCRETE WIENER INTERPOLATION

As shown in section 4.1.2.4, the CTF at the data positions can be written as

$$\widehat{\mathbf{h}}_d = \mathbf{A}\widehat{\mathbf{h}}_p \,, \tag{4.48}$$

where $\widehat{\mathbf{h}}_d = [\widehat{h}_{d1}\ \widehat{h}_{d2}\ ...\ \widehat{h}_{dd}]^T$ and $\widehat{\mathbf{h}}_p = [\widehat{h}_{p1}\ \widehat{h}_{p2}\ ...\ \widehat{h}_{pm}]^T$. It is assumed that there are d data and m pilot carriers. $\mathbf{A}$ is the weighting matrix shown in (4.35). This method can easily be applied to a mobile WiMAX system because discrete Wiener interpolation has the advantage of operating on data that is arbitrarily space. This implies that the estimated CTF at the carrier positions can be directly used to construct $\widehat{\mathbf{h}}_p$. The weighting matrix $\mathbf{A}$ is calculated using the same methodology as in section 4.1.2.4. The weights used to calculate the CFT at carrier i can be written as

$$\mathbf{A}_i = \mathbf{R}_{\mathbf{hh}}^{-\mathbf{1}}\mathbf{r}_{dwi} \,, \tag{4.49}$$

where $\mathbf{R}_{\mathbf{hh}} = E\{\mathbf{h}\mathbf{h}^H\}$ is the channel autocorrelation and $\mathbf{r}_{dwi}$ is the cross correlation of data symbol i with each of the pilot symbols.

4.2.3.4 ADAPTIVE LS INTERPOLATION

From (4.48) it can be seen that the CTF estimate at the data carriers is a function of the weighting matrix $\mathbf{A}$ and the pilot estimates. In this section it is demonstrated how the $\mathbf{A}$ matrix can be calculated by making use of previous observations and performing the method of LS. From Figure 4.9 it can be seen that the pilot positions varies for even and odd symbols for mobile WiMAX. This implies that the weight vector used to calculate the CTF at data carrier di $(\mathbf{w}_{di})$ as shown in (4.38) will be different for even and odd symbols. It follows that if N training symbols are transmitted, (4.36) for the even symbol case can be written as

$$\underbrace{\begin{bmatrix} \widehat{h}_{p1(2)} & \widehat{h}_{p2(2)} & \dots & \widehat{h}_{pm(2)} \\ \widehat{h}_{p1(4)} & \widehat{h}_{p2(4)} & \dots & \widehat{h}_{pm(4)} \\ \widehat{h}_{p1(6)} & \widehat{h}_{p2(6)} & \dots & \widehat{h}_{pm(6)} \\ \vdots & \vdots & \vdots & \vdots \\ \vdots & \vdots & \vdots & \vdots \\ \widehat{h}_{p1(N)} & \widehat{h}_{p2(N)} & \dots & \widehat{h}_{pm(N)} \end{bmatrix}}_{\mathbf{H}_{p(even)}\,(\frac{N}{2}\times m)} \underbrace{\begin{bmatrix} w_{1(di)} \\ w_{2(di)} \\ w_{3(di)} \\ \vdots \\ \vdots \\ w_{m(di)} \end{bmatrix}}_{\mathbf{w}_{di(even)}\ (m\times 1)} = \underbrace{\begin{bmatrix} \widehat{h}_{di(2)} \\ \widehat{h}_{di(4)} \\ \widehat{h}_{di(6)} \\ \vdots \\ \vdots \\ \widehat{h}_{di(N)} \end{bmatrix}}_{\mathbf{h}_{di(even)}\ (\frac{N}{2}\times 1)} . \tag{4.50}$$

Accordingly, (4.36) for the odd symbol case can be written as

$$\underbrace{\begin{bmatrix} \widehat{h}_{p1(1)} & \widehat{h}_{p2(1)} & \dots & \widehat{h}_{pm(1)} \\ \widehat{h}_{p1(3)} & \widehat{h}_{p2(3)} & \dots & \widehat{h}_{pm(3)} \\ \widehat{h}_{p1(5)} & \widehat{h}_{p2(5)} & \dots & \widehat{h}_{pm(5)} \\ \vdots & \vdots & \vdots & \vdots \\ \vdots & \vdots & \vdots & \vdots \\ \widehat{h}_{p1(N-1)} & \widehat{h}_{p2(N-1)} & \dots & \widehat{h}_{pm(N-1)} \end{bmatrix}}_{\mathbf{H}_{p(odd)}(\frac{N}{2}\times m)} \underbrace{\begin{bmatrix} w_{1(di)} \\ w_{2(di)} \\ w_{3(di)} \\ \vdots \\ \vdots \\ w_{m(di)} \end{bmatrix}}_{\mathbf{w}_{di(odd)}\ (m\times 1)} = \underbrace{\begin{bmatrix} \widehat{h}_{di(1)} \\ \widehat{h}_{di(3)} \\ \widehat{h}_{di(5)} \\ \vdots \\ \vdots \\ \widehat{h}_{di(N-1)} \end{bmatrix}}_{\mathbf{h}_{di(odd)}\ (\frac{N}{2}\times 1)} . \tag{4.51}$$

It should be noted that N in (4.50) and (4.51) is assumed to be an even number and that the estimates obtained at the data carriers $[\widehat{h}_{di(1)}\ \widehat{h}_{di(2)}\ \widehat{h}_{di(3)}\ \dots\ \widehat{h}_{di(N)}]$ are calculated in the same manner as the estimates at the pilot carriers. The weighting vector for data symbol $\mathbf{w}_{di(even)}$ and $\mathbf{w}_{di(odd)}$ can be calculated using the same methodology as presented in section 4.1.2.5 as

$$\mathbf{w}_{di(even)} = (\mathbf{H}^H_{p(even)}\mathbf{H}_{p(even)})^{-1}\mathbf{H}^H_{p(even)}\mathbf{h}_{di(even)}\ , \tag{4.52}$$

and

$$\mathbf{w}_{di(odd)} = (\mathbf{H}^H_{p(odd)}\mathbf{H}_{p(odd)})^{-1}\mathbf{H}^H_{p(odd)}\mathbf{h}_{di(odd)}\ . \tag{4.53}$$

From (4.50) and (4.51) it can be seen that the dimension of the $\mathbf{H}_{p(even)}$ and $\mathbf{H}_{p(even)}$ matrices is $\frac{N}{2}\times m$. This implies that if N training symbols are transmitted, half of the symbols will be used to calculate $\mathbf{w}_{di(even)}$ while the other half will be used to calculate $\mathbf{w}_{di(odd)}$.

4.3 CONCLUSION

In this chapter, several channel estimation methods for mobile WiMAX were discussed. It was shown that classical block type OFDM channel estimation can be used to obtain a channel estimate on the preamble. Comb type OFDM channel estimation on the other hand can be used to perform channel estimation on mobile WiMAX data symbols. A MST TD LS estimation method was proposed for preamble channel estimation while an adaptive LS estimation algorithm was proposed for use on mobile WiMAX PSAM data symbols. In the following chapter, the channel estimation methods proposed in this chapter are evaluated in terms of their performance using a mobile WiMAX simulation platform.

CHAPTER FIVE

RESULTS

In this chapter, the performance of the preamble as well as the PSAM based estimation methods presented in section 4.1.1 and 4.1.2 are evaluated on a mobile WiMAX simulation platform. In the case of preamble estimation, an estimation realization at various $\frac{E_b}{N_o}$ levels is presented for illustrative purposes followed by the BER performance analysis. In the case of PSAM estimation, all the FD interpolation methods discussed in section 4.1.2 are compared in terms of BER performance. The simulation parameters are constant for each group of simulations to ensure a fair comparison.

The simulation platform presented in chapter 3 was developed using the C++ programming language. Most of the algorithms implemented on the simulator were initially developed using a scaled down version of the simulator developed in MATLAB. The reason for this was to thoroughly test each algorithm before implementation on the main simulator. Simulations were done using the University of Pretoria's high performance cluster containing hundreds of individual CPU's running the Debian Linux operating system.

5.1 PREAMBLE CHANNEL ESTIMATION SIMULATION RESULTS

In this section, the simulation results for each of the preamble channel estimation methods presented in section 4.1.1 are shown. The simulation parameters are given in Table 5.1. The mobile WiMAX standard supports TDD, half duplex FDD as well as full duplex FDD mode of operation [9], however the initial release of mobile WiMAX certification profiles will only include TDD operating at 2.5 GHz [25, 51]. Accordingly the duplexing mode and carrier frequency was set at TDD and 2.5Ghz respectively. The only mandatory CP ratio specified in the mobile WiMAX standards is $\frac{1}{8}$, it follows that the CP length chosen for simulator was set accordingly. The complex fading channel induces a phase rotation as well as an amplitude shift on the transmitted symbol, this channel effect is mitigated by the use of a ZF equalizer discussed in chapter 4. When using a modulation scheme which uses variable amplitude as well as phase, the true value of equalization becomes apparent because the both the in-phase and quadrature-phase components are affected by the complex channel and needs to be corrected. For this reason for this reason 16QAM modulation, which has variable phase and amplitude, was chosen. The commonly accepted 1xEVDV evaluation methodology [52, 53] was adopted which uses the ITU-T ped. B Ch 103 multipath profile [20] *(see Appendix A)*.

There are 48 OFDMA symbols in a 5 ms frame [25] and most commonly half of the symbols are used for UL and half for DL. It follows that the number of DL OFDMA data symbols were consequently set to 24. Because most mobile radio systems operate in urban environments where a line of sight component is usually non existent [1], the fading amplitude was Rayleigh distributed and was simulated using the improved Jakes model [12].

When using preamble estimation, the channel estimate is made using only the preamble (which is first symbol of the DL frame) and is used to equalize the following symbols for the duration of the frame. This implies that the channel needs to remain constant for the duration of a the DL frame which in this case is 24 symbols. For this reason the velocity was set to 3 km/h.

Simulation parameter	Setting
WiMAX access scheme	OFDMA
Subchannel Allocation	FUSC
Number of carriers	128
Carrier Frequency	2.5 GHz
Cyclic Prefix Ratio	$\frac{1}{8}$
Velocity	3 Km/h
Modulation	16QAM
DL Data Symbols per Frame	24
Channel Profile	ITU-Ped B 103
Fading	Rayleigh
Duplexing Mode	TDD

TABLE 5.1: Preamble estimation simulation parameters

5.1.1 FD LS CHANNEL ESTIMATION

The FD LS estimation algorithm was applied to the WiMAX simulation platform as discussed in section 4.2.2.1. Figure 5.1 shows the effect of noise on the estimation accuracy of FD LS channel estimation. For illustrative purposes, a sample is shown of a channel estimate at 0, 5, 10 and 15 dB $\frac{E_b}{N_o}$. From this, the inherent susceptibility of FD LS estimation to noise is clearly demonstrated. Figure 5.2 shows the performance of the FD LS estimator compared to perfect CSI. It can be seen that there is approximately a 4 dB loss in the BER when using FD LS estimation which correspond with results given in [39, 54].

5.1.2 FD LMMSE CHANNEL ESTIMATION

The FD LMMSE estimation algorithm was applied to the WiMAX simulation platform as discussed in section 4.2.2.2. Figure 5.3 shows the effect of noise on the estimation accuracy. When compared to LS FD estimation it can be seen that effect of noise is much less dramatic. The power of the LMMSE algorithm can especially be seen at low $\frac{E_b}{N_o}$ values which correlates to results found in [21, 39, 43, 54, 55]. The noise robustness of the FD LMMSE algorithm is shown in Figure 5.4 where it can be seen that there is only a 0.5 dB difference at 1% BER when compared to prefect CSI. In section 4.2.2.2 it was shown that the autocorrelation of the channel $\mathbf{R_{hh}}$ is required when using the FD LMMSE channel estimation method. If a stochastic process is ergodic, time averages can be used to determine an approximation corresponding to the ensamble averages [56]. Provided that the realizations are

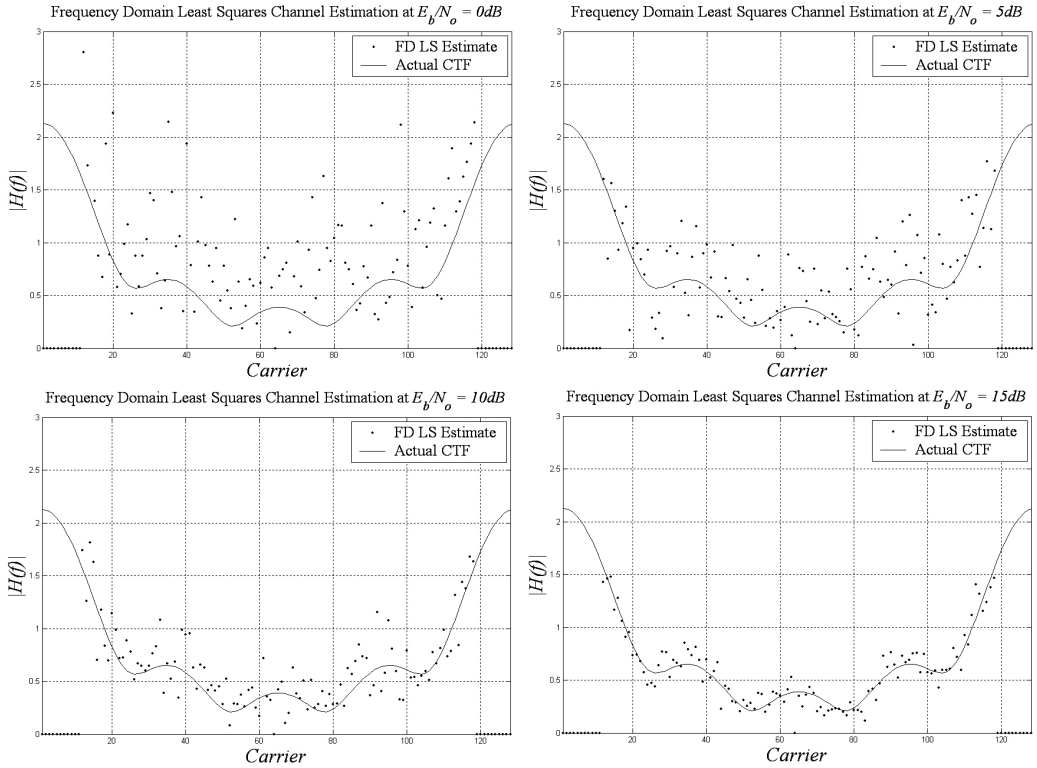

FIGURE 5.1: FD LS estimation at various $\frac{E_b}{N_o}$ levels

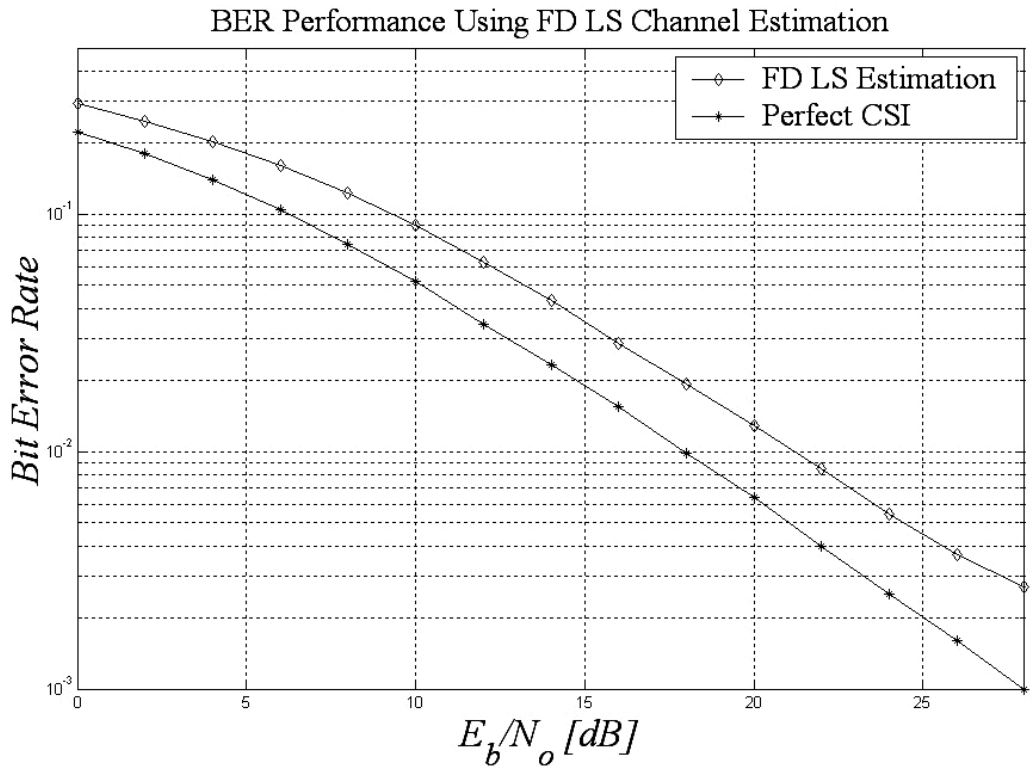

FIGURE 5.2: BER performance using FD LS estimation

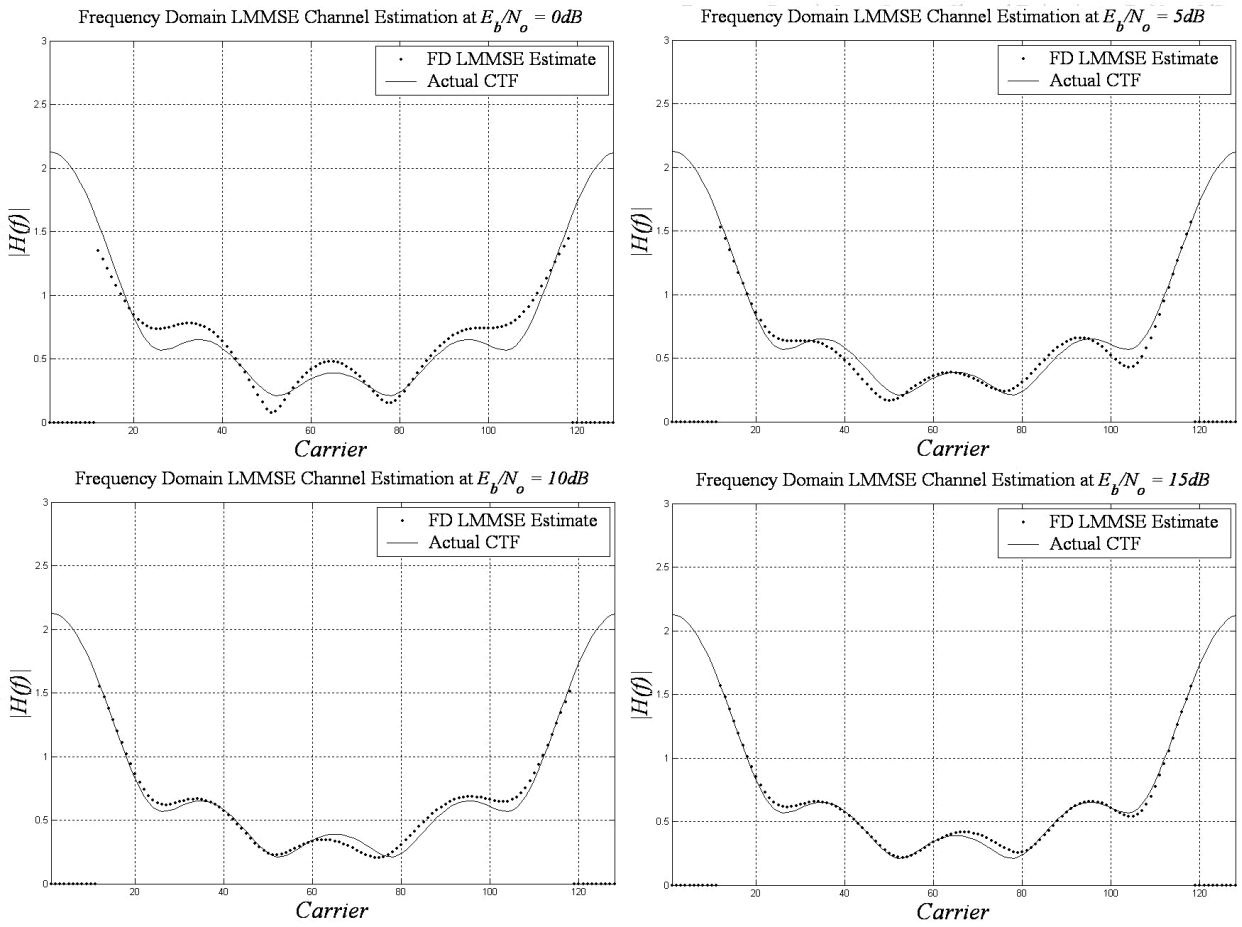

FIGURE 5.3: FD LMMSE estimation at various $\frac{E_b}{N_o}$ levels

sufficiently long in duration, the autocorrelation $\mathbf{R_{hh}}$ can be written as [42]

$$\mathbf{R_{hh}} = \lim_{N\to\infty} \frac{1}{N} \sum_{n=1}^{N} \mathbf{h}\mathbf{h}^H \ . \tag{5.1}$$

Based on (5.1), the value of $\mathbf{R_{hh}}$ used in simulating the performance of the FD LMMSE estimation method was obtained by means of Monte-Carlo simulation [39].

5.1.3 FD LS CHANNEL ESTIMATION WITH DFT IMPROVEMENT

The FD LS with DFT improvement estimation algorithm was applied to the WiMAX simulation platform as discussed in section 4.2.2.3. Figure 5.5 shows the effect of noise on the estimation accuracy. It can be seen that the effect of noise is not as detrimental at low $\frac{E_b}{N_o}$ values when compared to normal FD LS estimation. It can however also be seen that the estimation accuracy does not increase significantly at higher $\frac{E_b}{N_o}$ values if one considers for example 10 and 15 dB. This observation coincides with the BER graph in Figure 5.6 where it is shown that the BER performance only increases

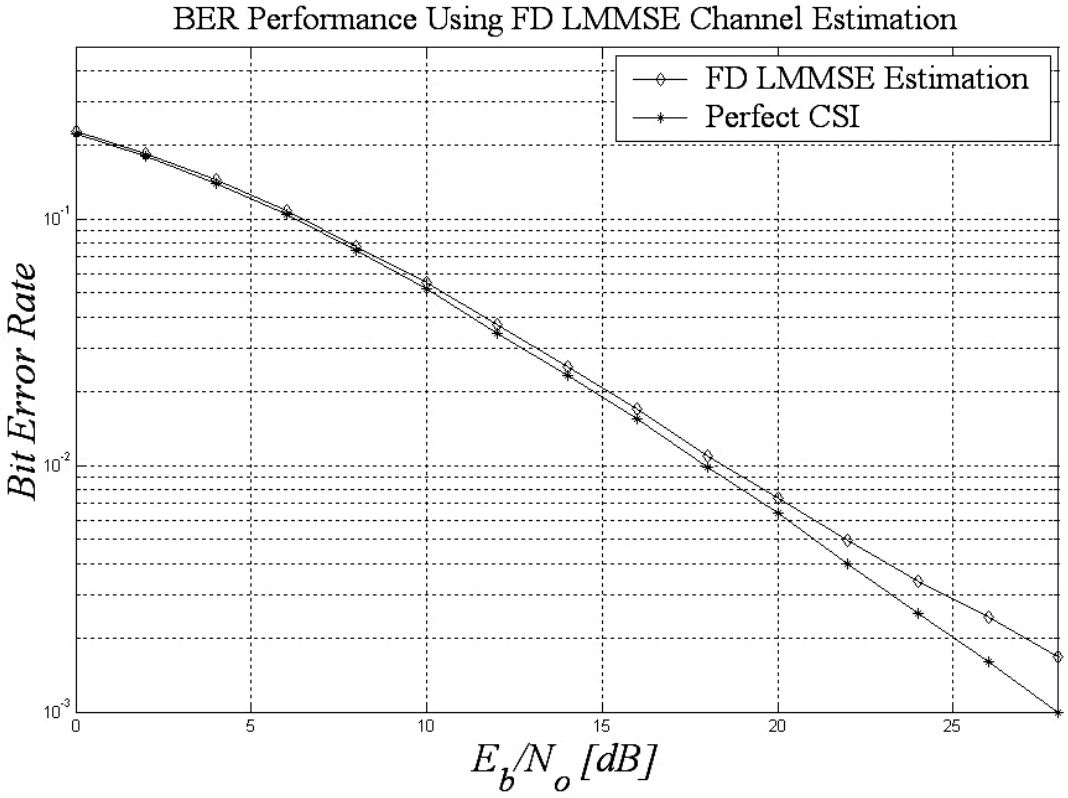

FIGURE 5.4: BER performance using FD LMMSE estimation

marginally at higher $\frac{E_b}{N_o}$ values. The reason for this is because of the systematic error induced by the PC interpolation on the guard bands (see section 4.2.2.3). In [41], it was shown that the systematic error induced by interpolation on the guard bands causes an eventual error floor when considering the BER performance. This corresponds with results found when testing the performance of the FD LS with DFT improvement algorithm on the WiMAX platform.

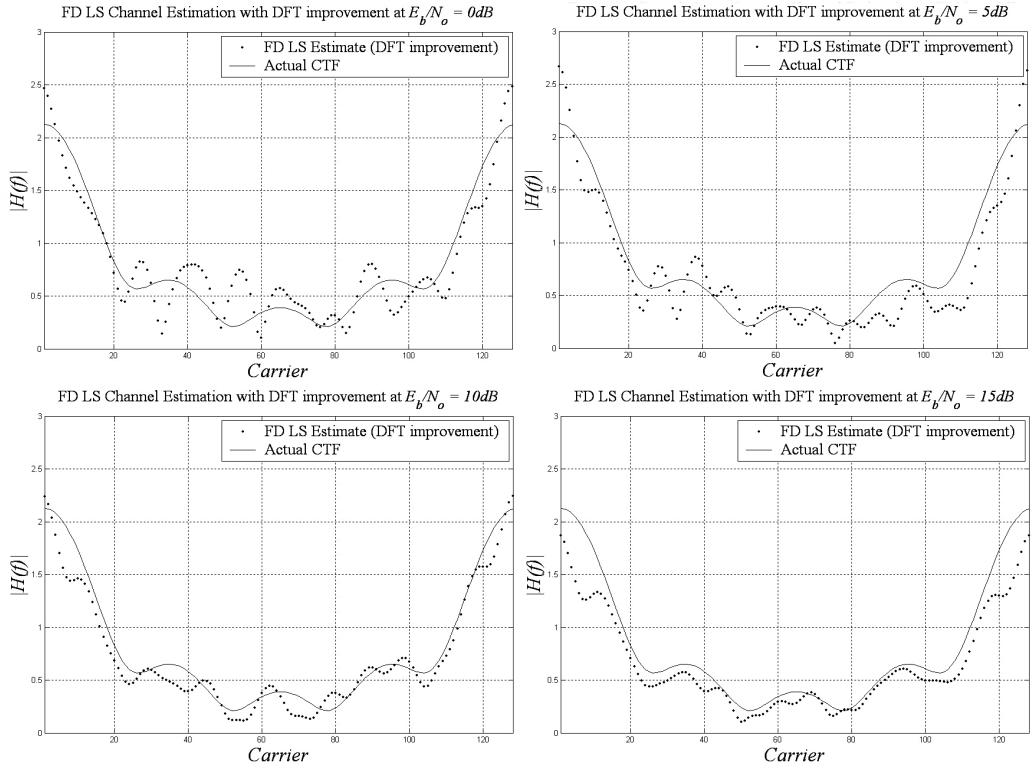

FIGURE 5.5: FD LS estimation with DFT improvement at various $\frac{E_b}{N_o}$ levels

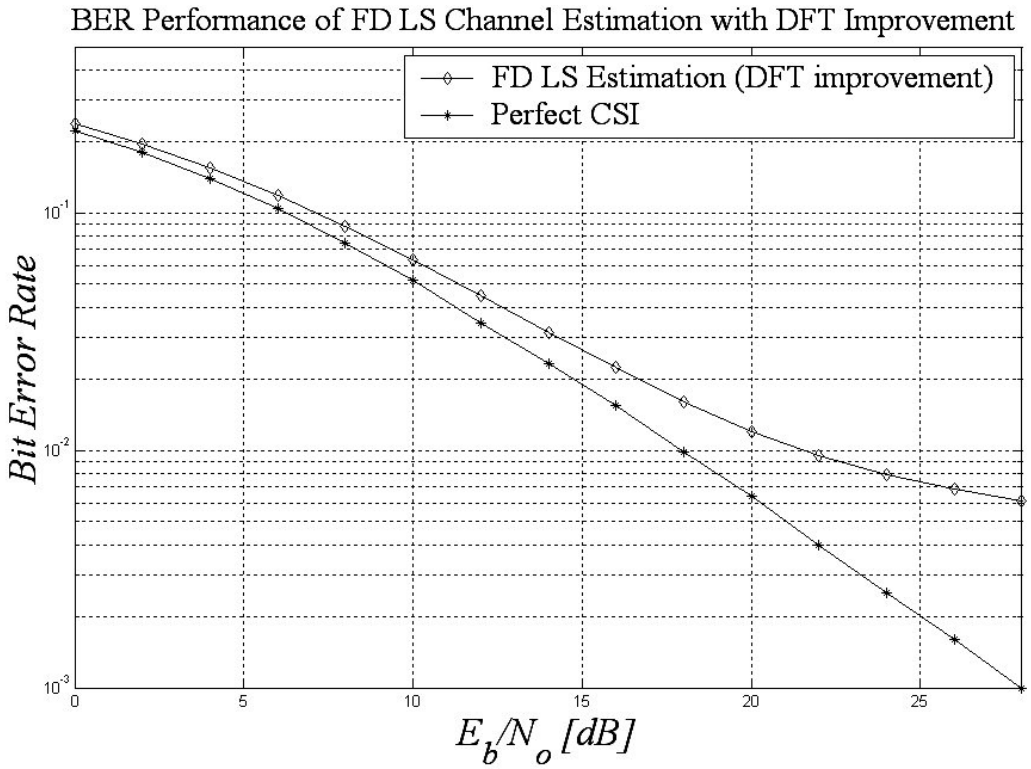

FIGURE 5.6: BER performance using FD LS estimation with DFT improvement

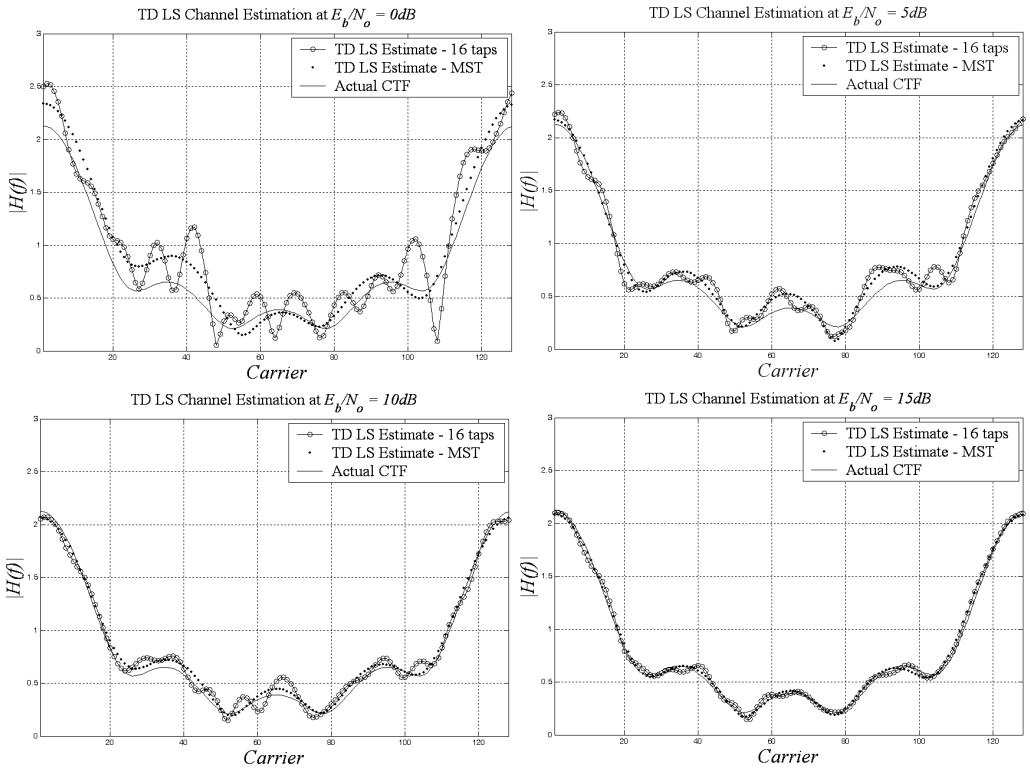

FIGURE 5.7: TD LS estimation at various $\frac{E_b}{N_o}$ levels

5.1.4 TD LS CHANNEL ESTIMATION

The TD LS estimation algorithm was applied to the WiMAX simulation platform as discussed in section 4.2.2.4. Figure 5.7 gives an illustration of the performance of the algorithm under varying noise conditions for the standard TD LS channel estimation using the CP length as well as the MST method. It can be observed that the fluctuation of the TD LS estimate using 16 taps is much higher than that of the estimate using the MST method. The reason for this is that when estimating 16 taps, the noise perturbation from the taps that carry no energy causes an inaccuracy in the frequency domain. This coincides with the BER performance in Figure 5.8 where the performance of MST algorithm proposed in section 4.1.1.4 shows a 0.5 dB improvement in performance at 1% BER over the standard CP length TD LS channel estimator.

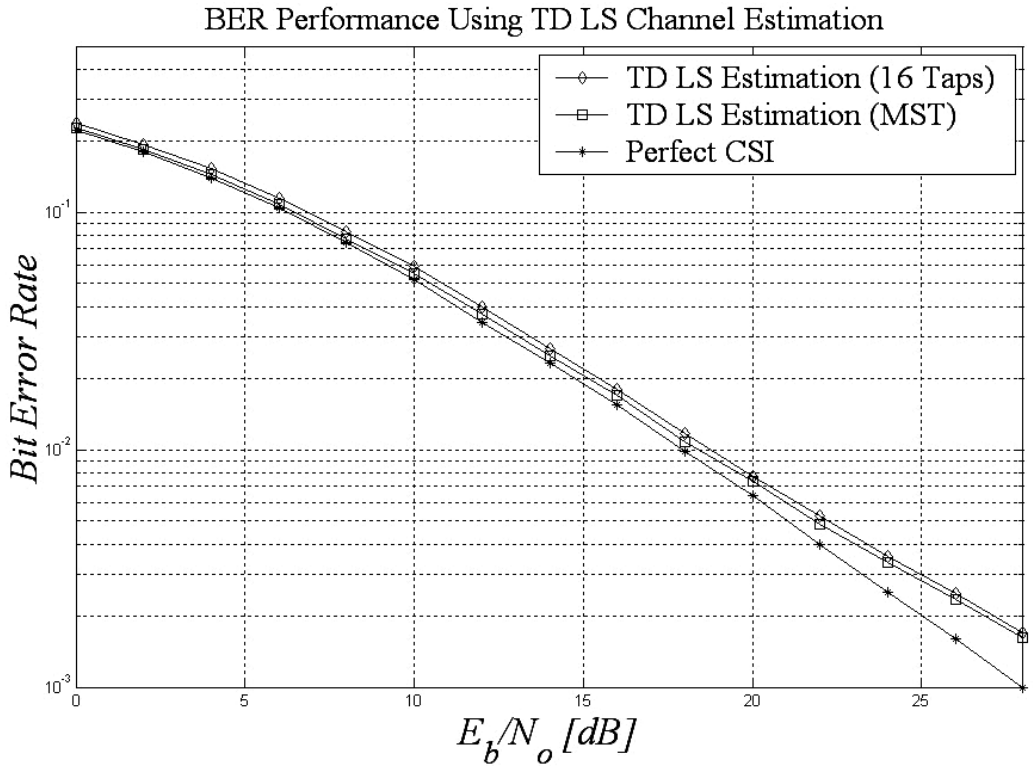

FIGURE 5.8: BER performance using TD LS estimation

5.1.5 COMPARISON OF PREAMBLE BASED ESTIMATION METHODS

Figure 5.9 shows the BER performance comparison of all the preamble estimation methods discussed in chapter 4. From the results it can seen that in the $\frac{E_b}{N_o}$ range of between 0 and 20 dB , FD LS estimation has the worst performance followed by FD LS estimation with DFT improvement, TD LS estimation (16 Taps), FD LMMSE and TD LS estimation (MST). The performance of the proposed MST TD LS estimation method performed marginally better than FD LMMSE estimation as shown in Figure 5.10 where the BER graph was zoomed in at an $\frac{E_b}{N_o}$ value of 20 dB. The reason for this is that even though TD LS estimation does not utilize the channel autocorrelation and noise variance, the number of most significant taps in the time domain is far less than the number of FD channel taps, thus requiring fewer parameters to estimate given the same amount of data. In the $\frac{E_b}{N_o}$ region of 20 dB upwards, it was found that normal FD LS estimation outperformed FD LS estimation with DFT improvement. This is because of the induced systematic error caused by interpolation on the guard bands when using the FD LS method with DFT improvement (see section 5.1.3).

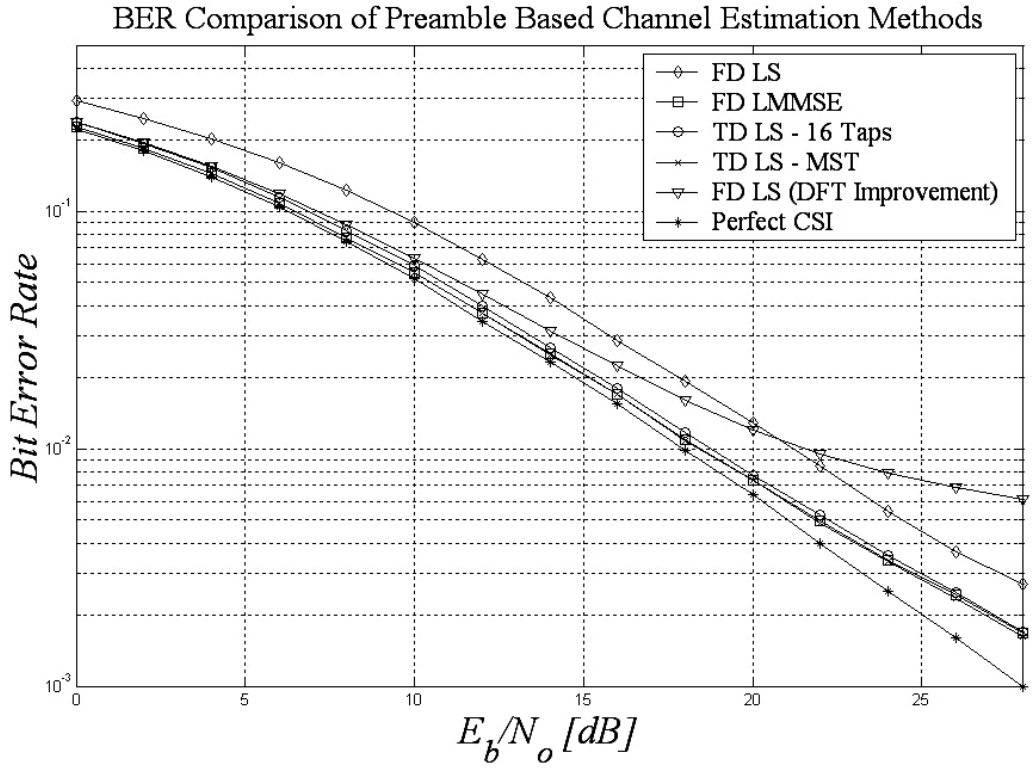

FIGURE 5.9: BER comparison of preamble based estimation methods

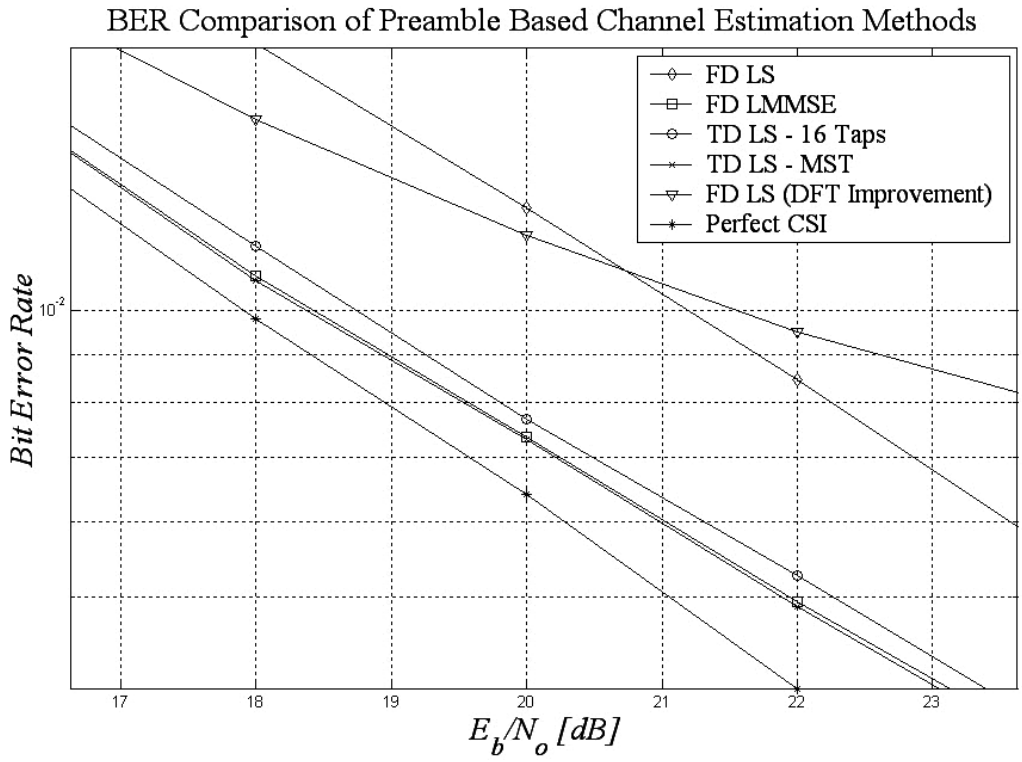

FIGURE 5.10: BER comparison of preamble based estimation methods at 20 dB

Simulation parameter	Setting
WiMAX access scheme	OFDMA
Subchannel Allocation	FUSC
Number of carriers	128
Carrier Frequency	2.5 GHz
Cyclic Prefix Ratio	$\frac{1}{8}$
Velocity	60 Km/h
Modulation	16 QAM
DL Data Symbols per Frame	24
Channel Profile	ITU-Ped B 103
Fading	Rayleigh
Duplexing Mode	TDD

TABLE 5.2: PSAM estimation simulation parameters

5.2 PSAM CHANNEL ESTIMATION SIMULATION RESULTS

In this section, the simulation results for each of the PSAM channel estimation methods presented in section 4.1.2 are shown. The simulation parameters that were used can be seen in Table 5.2. The parameters were identical to those used for preamble channel estimation in section 5.1 except for the mobile speed which was set to 60 km/h. With PSAM estimation, a channel estimate is made for each data symbol which implies that the channel only needs to be constant for one data symbol as opposed to the entire DL frame as is the case with preamble channel estimation. To ensure that the channel could be regarded as being quasi-static the mobile velocity was limited to 60 Km/h as suggested in [57]. In the following sections, the BER performance of the PC, linear, spline cubic, discrete Wiener and Adaptive LS interpolation methods implemented on a mobile WiMAX simulation platform are shown.

5.2.1 PIECEWISE CONSTANT, LINEAR AND SPLINE CUBIC INTERPOLATION

The PC, linear and spline cubic FD interpolation methods were applied to the WiMAX simulation platform as discussed in sections 4.1.2.1, 4.1.2.2 and 4.2.3.2 respectively. The BER comparison of these methods can be seen in Figure 5.11. As expected, linear interpolation outperformed PC interpolation while spline cubic interpolation yielded the best performance of the three methods. The performance superiority of linear interpolation over PC interpolation corresponds with similar performance comparisons done in [58]. The error floor experienced by all three methods is due to the systematic error discussed in sections 4.1.2.1, 4.1.2.2 and 4.2.3.2.

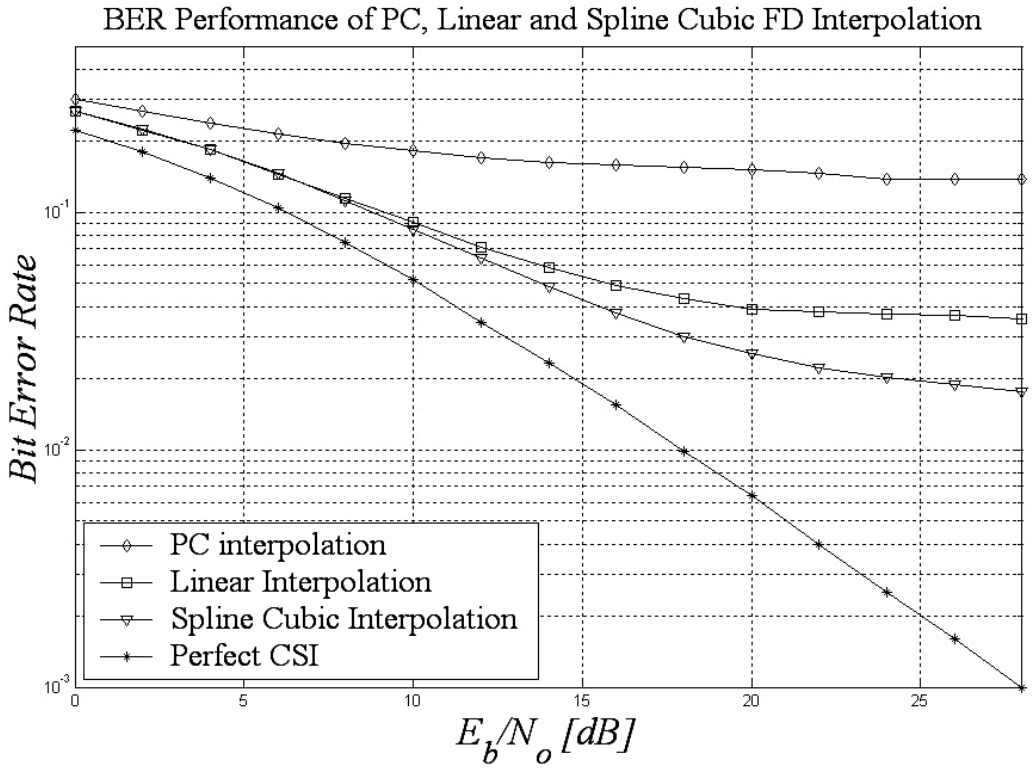

FIGURE 5.11: PC, linear and spline cubic FD interpolation

5.2.2 DISCRETE WIENER AND ADAPTIVE LS INTERPOLATION

As shown in section 4.1.2.4, discrete Wiener interpolation is optimal when considering the MSE. This interpolation scheme uses second order statistics assumed to be known *a-priori* to calculate a weighting matrix. This weighting matrix is then multiplied with the pilot estimates to obtain the channel response at data carriers. In section 4.1.2.5, a method was proposed to determine this weighting matrix deterministically by making use of the method of LS using previously transmitted fully known pilot symbols. The performance of the discrete Wiener as well as the adaptive LS interpolation schemes are compared in Figure 5.12. The number of observations used in the adaptive LS method were 400, 800 and 1200 symbols respectively. It should be noted that the pilot structure of mobile WiMAX is different for even and odd symbols which implies that half of the total number of training symbols were used to train the odd and even weighting matrix respectively (see section 4.2.3.4). From Figure 5.12, it can be seen that the performance of the LS training method is significantly influenced by the number of training symbols used. It was found that using more than 1200 had a negligible improvement in the performance of the proposed adaptive LS method. When considering a BER of 1%, it was found that the performance of the adaptive LS algorithm comes within 0.2 dB of optimal discrete Wiener interpolation.

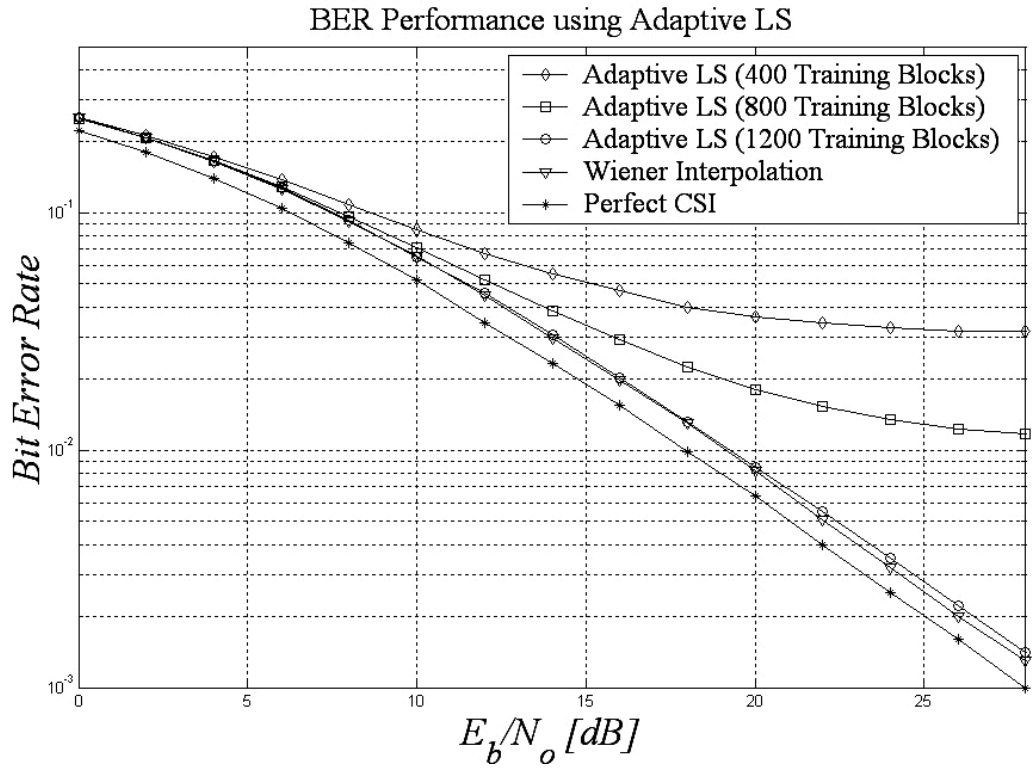

FIGURE 5.12: Discrete Wiener and adaptive LS interpolation

5.2.3 COMPARISON OF PSAM BASED ESTIMATION METHODS

In this section, the PSAM based estimation methods are compared with one another. Figure 5.13 shows the BER as a function of $\frac{E_b}{N_o}$ for all the different FD interpolation methods. It can be seen that PC, linear and spline cubic interpolation suffers from a systematic error induces error floor which corresponds to results found in [58, 59]. As expected, discrete Wiener interpolation yielded the best results, closely followed by the proposed adaptive LS method using 1200 training symbols. When using 800 training symbols, the adaptive LS interpolation method outperformed spline cubic, linear as well as PC interpolation. The adaptive LS method using 400 training blocks shows a slight performance increase over linear interpolation.

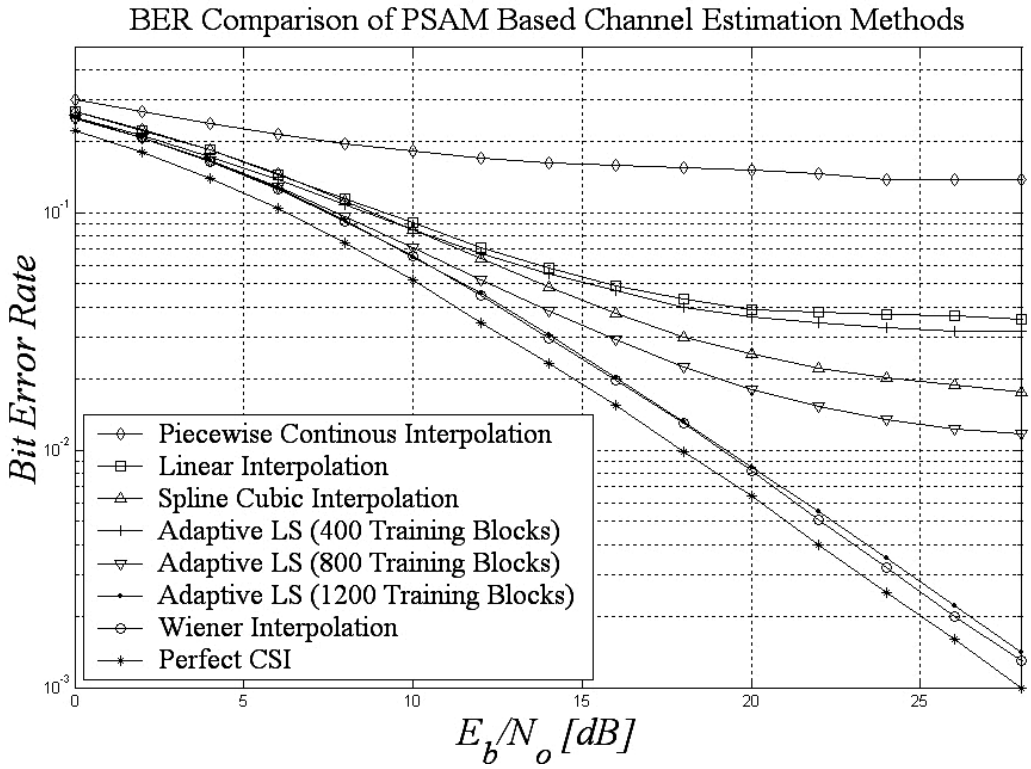

FIGURE 5.13: Comparison of PSAM estimation methods

5.3 CONCLUSION

In this chapter, several channel estimation methods focusing on preamble and PSAM estimation respectively were evaluated in detail and compared with one another using a mobile WiMAX simulation platform developed as part of this dissertation. It was found that the proposed MST TD LS algorithm performed virtually identical to FD LMMSE but had reduced complexity and did not use any second order statistics.

When considering PSAM estimation, the optimality of Wiener interpolation was confirmed via simulation results. The use of second order statistics does however make this method very difficult to implement in a real world environment. It was shown that given enough symbol observations, the proposed adaptive LS method came within fractions of a dB of optimal Wiener interpolation and outperformed PC, linear and spline cubic interpolation even when using 800 training symbols.

CHAPTER SIX

CONCLUSION AND FUTURE RESEARCH

6.1 CONCLUDING REMARKS

In this dissertation, several channel estimation methods for mobile WiMAX were analyzed and evaluated using a mobile WiMAX simulation platform developed as part of this dissertation. It was shown in chapter 3 that the access scheme of choice used in mobile WiMAX is OFDMA which is based on the concept of OFDM.

Estimation methods typically used in classical OFDM block-type pilot insertion, which included FD LS, FD LMMSE, FD LS with DFT improvement as well as TD LS were adapted to perform channel estimation using the preamble in a mobile WiMAX system. A method was proposed to improve on standard TD LS estimation by making use of a MST approach. It was shown in chapter 5 that the performance of this proposed method is virtually identical to FD LMMSE while having reduced complexity and no need for second order statistics.

Classical comb type FD interpolation methods, which included PC, linear, spline cubic and Wiener interpolation were adapted to perform channel estimation on the data symbols used in mobile WiMAX. An adaptive LS algorithm was also proposed. Wiener interpolation is optimal in the MSE sense, this was concurred by means of simulation as shown in chapter 5. The performance of the proposed Adaptive LS method did however perform fractionally poorer than optimal Wiener interpolation when using more than 1200 training OFDM symbols, when using 800 training symbols, the adaptive LS algorithm outperformed PC, linear as well as spline cubic interpolation.

As shown in chapter 3, the duration of a mobile WiMAX OFDMA symbol using a CP ratio of $\frac{1}{8}$ is 102.9μs. This relates to a training duration of 123ms and 82ms using 1200 and 800 training symbols

respectively. Assuming that the maximum access delay of the channel does not vary significantly, the weighting matrix used in the adaptive LS method will remain valid for an extended time period. This implies that frequent retraining will not be necessary.

6.2 FUTURE RESEARCH

The following are some of the possible areas that could be further investigated pertaining to channel estimation as well as simulation platform improvements for a mobile WiMAX system:

- The WiMAX simulation platform can be modified to include multiple input multiple output (MIMO) functionality which is already supported in the mobile WiMAX standard.
- The presented channel estimation methods could be extended to operate in a time and frequency direction, thus using the entire frame as opposed to a single OFDM symbol for estimation. These methods are typically referred to as 2D estimation methods.
- Based on the preamble channel estimate which is made using the first symbol of the TDD frame, channel tracking methods could be used to obtain the CIR for the entire frame
- Pre-equalization can be used when operating in TDD mode. This is done by convolving the transmitted TD symbol with the inverse of the channel estimate and transmitting the resulting symbol across the channel.

REFERENCES

[1] T. Rappaport, *Wireless Communications*. Upper Saddle River, NJ: Prentice Hall, 2002.

[2] D. Noble, "The history of land-mobile radio communications," *IEEE Transactions on Vehicular Technology*, vol. 50, no. 5, pp. 1405–1414, May 1962.

[3] V. MacDonald, "The cellular concept," *The Bell Systems Technical Journal*, vol. 58, no. 1, pp. 15–43, July 1979.

[4] Mobile WiMAX - part 2: A comparative analysis. [Online]. Available: http://www.wimaxforum.org/technology/downloads [Accessed: March 25, 2008]

[5] K. Santhi, V. Srivastava, G. Senthil, and A. Butare., "Goals of true broad bands wireless next wave (4G-5G)," in *IEEE Vehicular Technology Conference*, vol. 4, Oct. 2003, pp. 2317–2321.

[6] *IEEE standard Part 11: wireless LAN medium access control (MAC) and physical layer (PHY) specification.*, IEEE Amendment 3: specifications for operation in additional regulatory domains 802.11, 2001.

[7] Wimax forum. [Online]. Available: http://www.wimaxforum.org/ [Accessed: March 25, 2008]

[8] WiMAX planning : The AIRCOM perspective. [Online]. Available: http://www.aircom.co.uk/wimax [Accessed: March 25, 2008]

[9] *Air Interface for Fixed and Mobile Broadband Wireless Systems*, IEEE Amendment and Corrigendum to IEEE Std. 802.16-2004 802.16e-2005, 2005.

[10] J. Bingham, "Multicarrier modulation for data transmission: An idea whose time has come," *IEEE Communications Magazine*, pp. 5–14, May 1990.

[11] J. Proakis and M. Salehi, *Communication System Engineering*. Upper Sadle River, New Jersey: Prentice-Hall, 2002.

[12] Y. Zheng and C. Xiao, "Improved models for the generation of multiple uncorrelated Rayleigh fading waveforms," *IEEE Communications Letters*, vol. 6, no. 6, pp. 256–258, June 2002.

[13] J. Terry and J. Heiskala, *OFDM Wireless LANs: A Theoretical and Practical Guide*, C. Bowers, Ed. Indianapolis, Indiana USA: SAMS Publishing, 2001.

[14] B. R. Saltzberg, "Performance of an efficient parallel data transmission system," *IEEE Transactions on Communications*, vol. 15, pp. 805–811, Dec. 1967.

[15] S. B. Weinstein and P. M. Ebert, "Data transmission by frequency-division multiplexing using the discrete Fourier transform," *IEEE Transactions on Communications*, vol. 19, pp. 628–634, Dec. 1971.

[16] S. Mitra, *Digital Signal Processing*, W. Stephen, Ed. New York, NY: McGraw Hill, 2002.

[17] *Air Interface for Fixed Broadband Wireless Systems*, IEEE Std. 802.16-2004, 2004.

[18] J. Cavers, "An analysis of pilot symbol assisted modulation for Rayleigh fading channels," *IEEE Transactions on Vehicular Technology*, vol. 40, no. 4, pp. 686–693, Nov. 1991.

[19] B. Sklar, "Rayleigh fading channels in mobile digital communication channels part 1 : Characterization," *IEEE Communications Magazine*, vol. 35, pp. 61–66, July 1997.

[20] *Feasibility Study of OFDM for UTRAN enhancement*, 3GPP Std. 3GPP TR 25.892 v0.2.0 (2003-03), 2003.

[21] Y. Li, L. Cimini, and N. Sollenberger, "Robust channel estimation for OFDM systems with rapid dispersive fading channels," *IEEE Transactions on Communications*, vol. 46, no. 7, pp. 902–915, July 1998.

[22] J. W. C. Jakes, *Microwave Mobile Communications*. New York, N.Y. USA: John Wiley and Sons, 1974.

[23] P. Chen and H. Kobayashi, "Maximum likelihood channel estimation and signal detection for OFDM systems," in *IEEE International Conference on Communication*, Apr. 2002, pp. 1640–1645.

[24] R. M. Gray, "Toeplitz and circulant matrices: A review," Department of Electrical Engineering, Stanford University, Stanford, USA, Tech. Rep.

[25] "Mobile WiMAX Part I:A Technical Overview and Performance Evaluation," White Paper, Wimax Forum, Aug. 2006.

[26] E. Agis *et al.*, "Global, interoperable broadband wireless networks: Extending WiMAX technology to mobility," *Intel Technology Journal*, vol. 8, no. 3, pp. 173–187, Aug. 2004.

[27] I. Koffman and V. Roman, "Broadband wireless access solutions based on OFDM access in IEEE 802.16," *IEEE Communications Magazine*, pp. 96–103, Apr. 2002.

[28] J. Khun-Jush, P. Schramm, U. Wachsmann, and F. Wenger, "Structure and performance of the HIPERLAN/2 physical layer," in *IEEE Vehicular Technology Conference*, Amsterdam, Netherlands, June 1999, pp. 2667–2671.

[29] J. Lang and K. Lee, "Transmit power adaption for multiuser OFDM systems," *IEEE Journal on Selected Areas of Communication*, vol. 21, pp. 171–178, Feb. 2003.

[30] H. Yaghoobi, "Scalable OFDMA physical layer in IEEE 802.16 wireless MAN," *Intel Technology Journal*, vol. 8, no. 3, pp. 201–212, Aug. 2004.

[31] I. Kalet, "The multitone channel," *IEEE Transactions on Communications*, vol. 37, pp. 119–124, Feb. 1989.

[32] T. Willink and P. Wittke, "Optimization and performance evaluation of multicarrier transmission," *IEEE Transactions on Information Theory*, vol. 43, no. 2, pp. 426–440, Mar. 1997.

[33] B. Wichmann and D. Hill, "Building a random-number generator," *Byte Magazine*, pp. 127–128, Mar. 1987.

[34] G. Forney, "Maximum-likelihood sequence estimation of digital sequences in the presence of intersymbol interference," *IEEE Transactions on Information Theory*, vol. IT-18, no. 3, pp. 363–378, 1972.

[35] T. Roman, M. Enescu, and V. Koivunen, "Time-domain method for tracking dispersive channels in OFDM systems," in *The 57th IEEE Semiannual Conference on Vehicular Technology*, Apr. 2003, pp. 1318–1321.

[36] H. Van Trees, *Detection, Estimation and Modulation Theory*. New York, N.Y. USA: John Wiley and Sons, 2001.

[37] Y. Shen and E. Martinez, "Channel estimation in OFDM systems," *Freescale Semiconductors*, Jan. 2006.

[38] X. Hou, X. Zhao, C. Yin, and G. Yue, "Unified view of channel estimation in MIMO OFDM systems," in *International Conference on Wireless Communications, Networking and Mobile Computing*, Montreal, Sept. 2005, pp. 54–58.

[39] J. van de Beek et al., "On channel estimation in OFDM systems," in *Proc 45th IEEE Vehicular Technology Conference*, Chicago, IL, July 1995, pp. 815–819.

[40] Y. Zhao and A. Huang, "A novel estimation method for OFDM mobile communication systems based on pilot signals and transform domain processing," in *The 47th IEEE Conference on Vehicular Technology*, May 1997, pp. 2089–2093.

[41] Z. Cheng and D. Dahlhaus, "Time versus frequency domain channel estimation for OFDM systems with antenna arrays," in *6th International Conference on Signal Processing*, Beijing, Aug. 2002, pp. 1340–1343.

[42] S. Haykin, *Adaptive Filter Theory*, T. Kailath, Ed. Englewood Cliffs, New Jersey: Pretence-Hall, 1986.

[43] O. Edfors, M. Sandell, J.-J. van de Beek, S. K. Wilson, and P. O. Borjesson, "OFDM channel estimation by singular value decomposition," *IEEE Transactions on Communications*, vol. 46, no. 7, pp. 931–939, July 1998.

[44] H. Minn and V. Bharagava, "An investigation into time-domain approach for OFDM channel estimation," *IEEE Transactions on Broadcasting*, vol. 46, no. 4, pp. 240–248, Dec. 2000.

[45] B. Yang, K. Letaief, R. Cheng, and Z. Cao, "Channel estimation for OFDM transmission in multipath fading channels based on parametric channel modeling," *IEEE Transactions on Communications*, vol. 49, no. 3, pp. 467–478, Mar. 2001.

[46] G. Steward, *Introduction to Matrix Computations*. Academic Press, New York, 1973.

[47] M. F.-G. Garcia, J. Paez-Borrallo, and S. Zazo, "DFT-based channel estimation in 2d-pilot-symbol-aided OFDM wireless systems," in *The 53rd IEEE Conference on Vehicular Technology*, Rhodes, May 2001, pp. 810–814.

[48] S. Coleri, M. Ergen, A. Puri, and A.Bahai, "Channel estimation techniques based on pilot arrangement in OFDM systems," *IEEE Tranactions on Broadcasting*, vol. 48, no. 3, pp. 223–229, Sept. 2002.

[49] C. S. Yeh and Y. Lin, "Channel estimation using pilot tones in OFDM systems," *IEEE Tranactions on Broadcasting*, vol. 45, no. 4, pp. 400–409, Dec. 1999.

[50] J. Rinne and M. Renfors, "Pilot spacing in orthogonal frequency division multiplexing systems on practical channels," *IEEE Transactions on Consumer Electronics*, vol. 42, no. 4, pp. 959–1343, Nov. 1996.

[51] D. Wiggill, private communication, Redline Communications, 2006.

[52] "System-level evaluation of OFDM - further considerations," R1-031303, 3GPP TSG-RAN-1, Nov. 2003.

[53] "Effective SIR computation for OFDM system-level simulations," Meeting No. 35, 3GPP TSG-RAN-1, Lisbon, Portugal, Nov. 2003.

[54] Y. Shen and E. Martinez, "Channel estimation in OFDM systems," Freescale Semiconductor, Tech. Rep. AN3059.

[55] M. Chang, "A new derivation of least-squares-fitting principle for OFDM channel estimation," *IEEE Transactions on Wireless Communications*, vol. 5, no. 4, pp. 726–731, Apr. 2006.

[56] A. Papoulis, *Probability, Random Variables and Stochastic Processes*. New York: McGraw-Hill, 1984.

[57] WiMAX system overview poster. [Online]. Available: http://www.rohde-schwarz.com/ [Accessed: March 25, 2008]

[58] M. Hsieh and C. Wei, "Channel estimation for OFDM systems based on comb-type pilot arrangement in frequency selective fading channels," *IEEE Transactions on Consumer Electronics*, vol. 44, no. 1, pp. 219–225, Feb. 1998.

[59] M. Chang and Y. Su, "2D regression channel estimation for equalizing OFDM signals," in *51st Conference Proceedings on Vehicular Technology*, Tokyo, May 2000, pp. 240–244.

[60] D. Gray, "Mobile WiMAX - part 1: A technical overview and performance evaluation," *WiMAX Forum*, Feb. 2006.

[61] K. Jeong *et al.*, "Multipath channel models for wireless local and metropolitan area networks," in *Information Technology and Applications (ICITA)*, July 2005, pp. 295–298.

APPENDIX A
CHANNEL DELAY PROFILES

This section provides the ITU Channel 103 power delay profile (shown in Figure A.6) that is typically used when simulating mobile WiMAX systems [4, 20, 60]. To confirm the validity of this channel model, a number of channel delay profiles for various terrestrial environments operating in the 2.3 GHz band [61] is also shown in Figures A.1 to A.5. Table A.1 gives the maximum delay spread, average delay as well as the RMS delay for each of the channel models presented in [61]. The maximum delay spread was calculated as the time during which the multipath energy falls within 25 dB below the maximum as suggested in [1]

Environment	**Maximum Delay Spread [ns]**	**Average Delay [ns]**	**RMS Delay [ns]**
Rural	1690	86.55	235.8
Suburban	3070	437.32	618.93
Hilly	3280	332.18	562.13
Urban high-rise	3890	466.06	572.34
Urban rooftop	5280	379.48	702.48
Average	**3095**	**340.31**	**538.34**

TABLE A.1: Summary of power delay profiles

Environment	**Maximum Delay Spread [ns]**	**Average Delay [ns]**	**RMS Delay [ns]**
ITU Channel 103	3700	408.50	633.15

TABLE A.2: ITU channel 103 summary

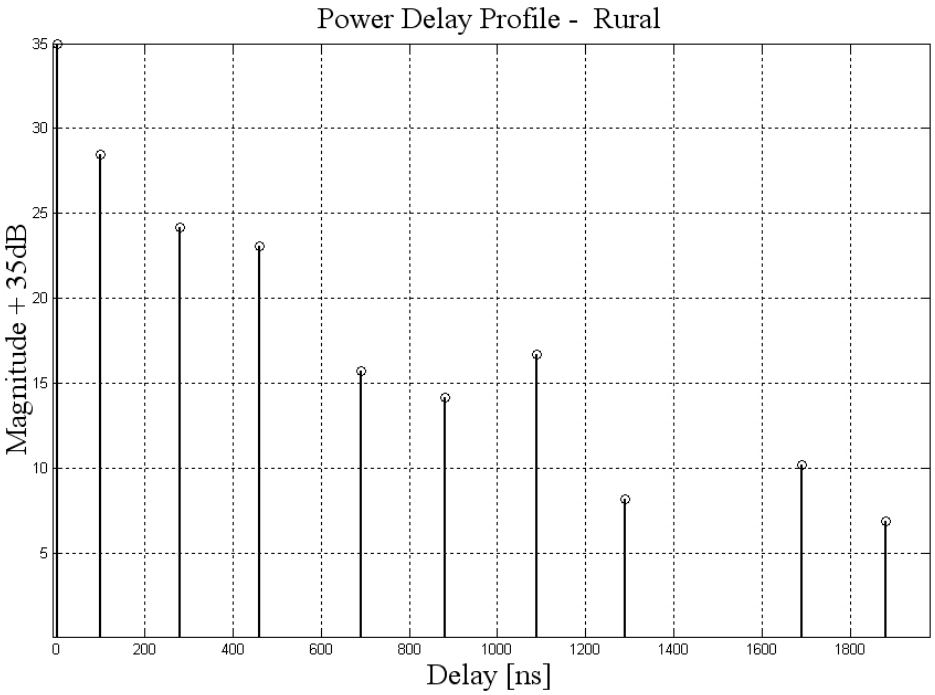

FIGURE A.1: PDP - Rural

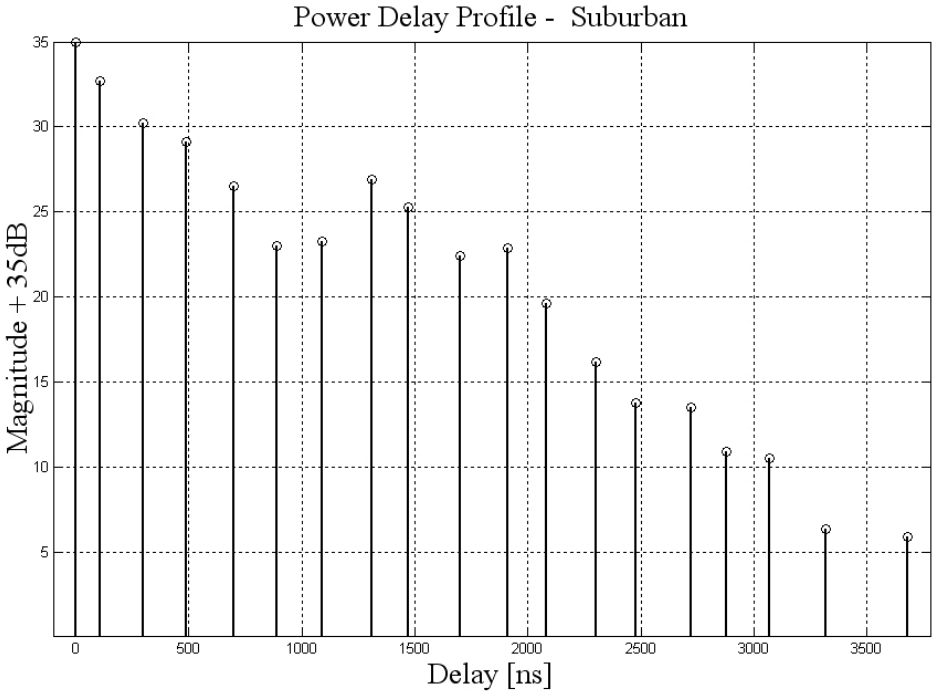

FIGURE A.2: PDP - Suburban

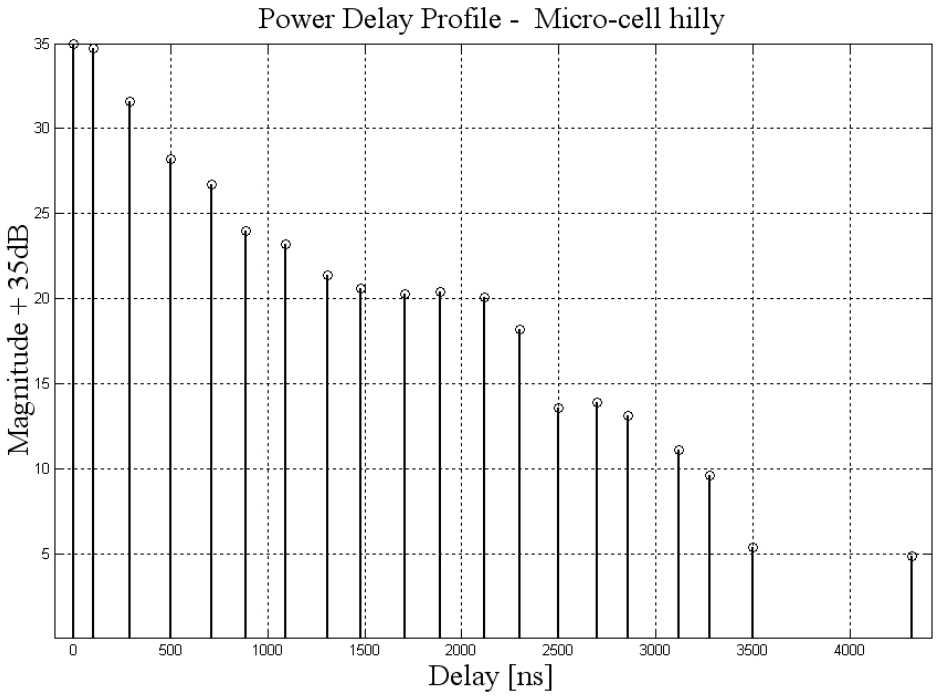

FIGURE A.3: PDP - Microcell Hilly

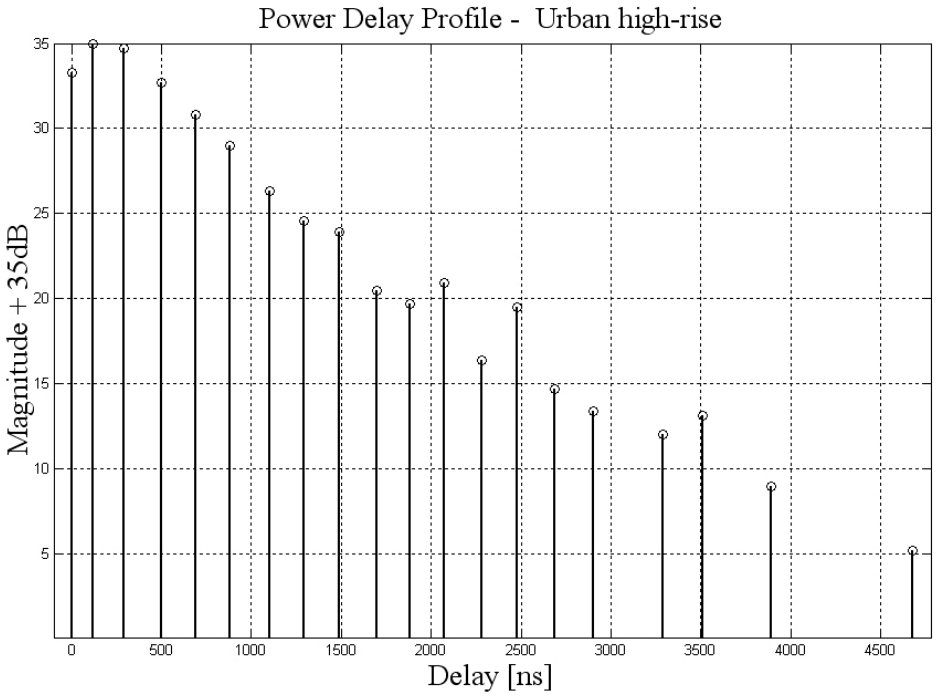

FIGURE A.4: PDP - Urban Highrise

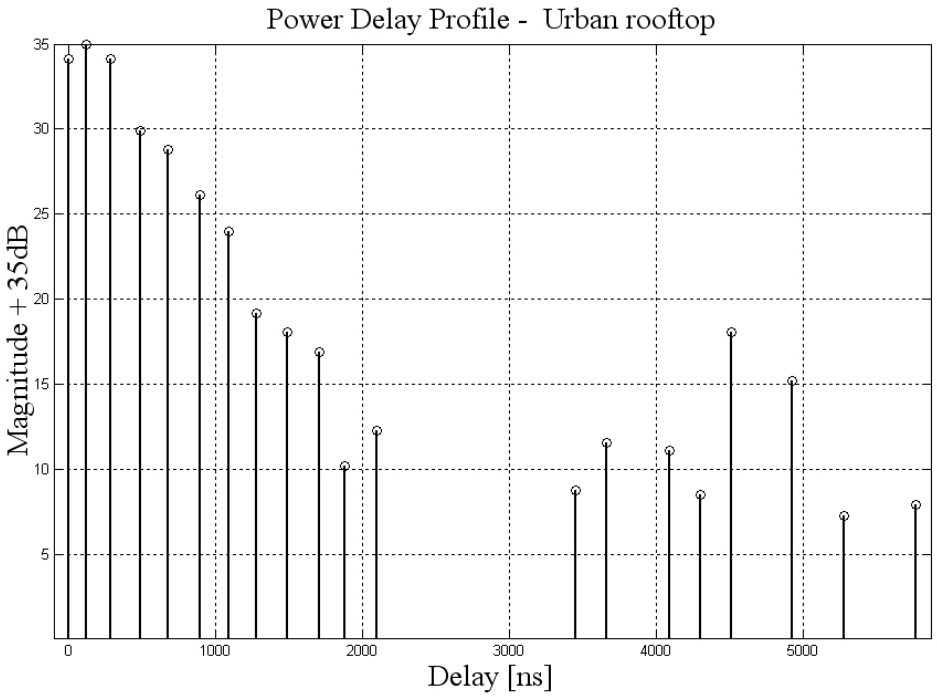

FIGURE A.5: PDP - Urban Rooftop

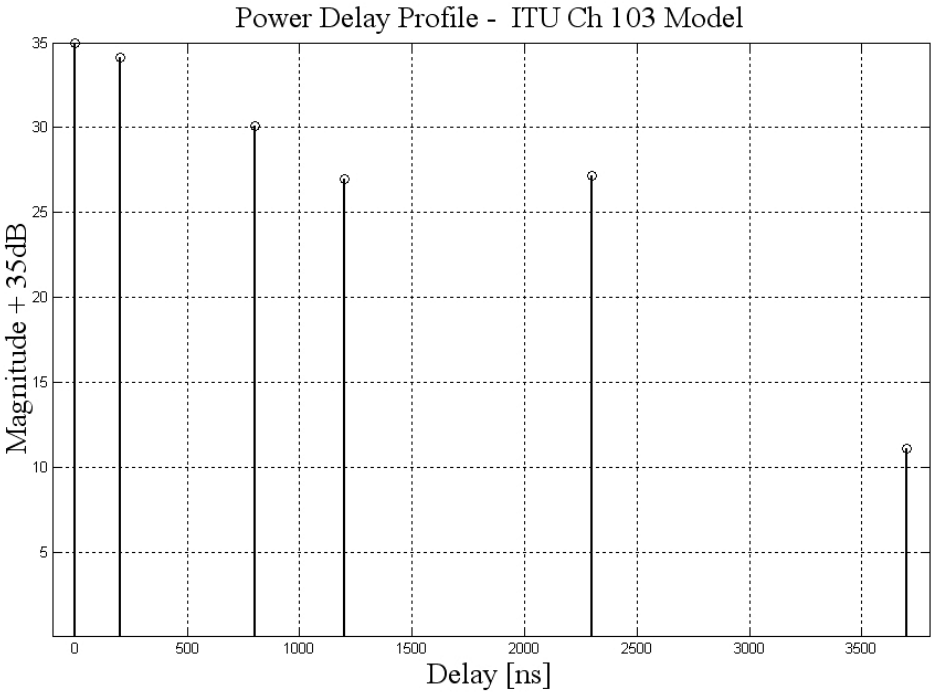

FIGURE A.6: PDP - ITU Channel 103